The Kearney ecosystem model
Kelly A. Kearney[1] and Charles Stock[2]

[1]Cooperative Institute for Marine and Atmospheric Studies, University of Miami Rosenstiel School of Marine and Atmospheric Science, 4301 Rickenbacker Causeway Miami, FL 33149 (corresponding author: kkearney@rsmas.miami.edu)
[2]NOAA Geophysical Fluid Dynamics Laboratory, 201 Forrestal Road, Princeton, NJ 08540-6649

Contents

List of Tables

1 Introduction

The model described in this document is a fully-coupled physical, biogeochemical, and ecosystem model. The generic model framework consists of a simple physical water column model, within which I run a biological module that adds in all the biologically-relevant state variables to this physical model. I never gave this model (or set of models) a proper name; I have a personal aversion to the trend of unintelligible acronyms but nothing better ever came to mind. I generally refer to it by the names of the Matlab functions it uses: the physical model is `mixed_layer.m`, the ecosystem model is `wce.m` (for water column ecosystem... damn, and unpronounceable and uninformative acronym!), and the NPZ-only biological module that I use for some setup and comparison is `nemurokak.m` (my own variant of the popular NEMURO model, with my initials appended). Taken as a whole, I've just named the thing after myself, since that's how it shows up for citation purposes.

Earlier versions of this documentation have appeared as an appendix to my Ph.D. thesis (Kearney, 2012) and as supplementary material to an earlier journal article (Kearney et al., 2013). Since then, the model has continued to evolve, and likely will continue to do so. I've spent a lot of time pulling my own hair out in attempts to understand the inner workings of other people's models, so I'm trying to keep things as transparent as possible with my own little pet model. This document will likely continue to accompany any publications that use this model as supplementary material, since all of this is far too detailed to go into journal articles themselves.

The basic model framework is designed to be generic to any pelagic ocean ecosystem. But in practice, it requires a huge number of input variables and datasets, so its development has been very closely tied to the specifics of my test ecosystem, the eastern subarctic gyre of the Pacific Ocean. The parameters and input datasets used to run the model for that ecosystem are listed here in full.

2 The physical model

2.1 Model framework and equations

The mixed-layer model simulates the evolution of water column properties under specified forcing by wind, heat, and salinity forcing. Allowance is also made for currents via a depth-independent pressure acceleration. There are six physical state variables in the physical model formulation: U and V are the east to west and south to north current velocities, and T and S are the temperature and salinity. The turbulence closure scheme introduces the remaining two state variables; : q^2 is a turbulent quantity equal to twice the turbulent kinetic energy, and ℓ is a turbulent length scale. The evolution of these quantities are governed according to:

$$\frac{\partial U}{dt} - fV = -\frac{1}{\rho_0}\frac{\partial p}{\partial x} + \frac{\partial}{\partial z}K_M\frac{\partial U}{\partial z} - \epsilon U \tag{1}$$

$$\frac{\partial V}{dt} + fU = -\frac{1}{\rho_0}\frac{\partial p}{\partial y} + \frac{\partial}{\partial z}K_M\frac{\partial V}{\partial z} - \epsilon V \tag{2}$$

$$\frac{\partial q^2}{\partial t} = \frac{\partial}{\partial z}K_q\frac{\partial q^2}{\partial z} + 2K_M\left[\left(\frac{\partial U}{\partial z}\right)^2 + \left(\frac{\partial V}{\partial z}\right)^2\right] + \frac{2g}{\rho_0}K_H\frac{\partial \rho}{\partial z} - \frac{2q^3}{B_1\ell} \tag{3}$$

3

$$\frac{\partial q^2 \ell}{\partial t} = \frac{\partial}{\partial z} K_q \frac{\partial q^2 \ell}{\partial z} + E_1 \ell \left(K_M \left[\left(\frac{\partial U}{\partial z} \right)^2 + \left(\frac{\partial V}{\partial z} \right)^2 \right] + E_3 \frac{g}{\rho_0} K_H \frac{\partial \rho}{\partial z} \right) - \frac{q^3}{B_1} W \tag{4}$$

These equations are solved using a semi-implicit Crank-Nicolson scheme.

Boundary forcing for U and V are set by the wind and bottom stress (see Section 2.1.1 and Section 2.1.2). The depth-independent pressure acceleration terms is specified as part of the model forcing. The bottom stress generated by currents arising from this term help prevent the bottom layers of the water column from stagnating. A dissipation term is included in equation (**??**) and equation (**??**) as a surrogate for horizontal momentum divergence. This term removes energy from past storm events over a specified time-scale as though energy was being transferred to more quiescent surrounding waters. Energy tends to accumulate unrealistically in 1D water columns without this effect (Mellor, 2001). The value of ϵ can be tuned such that the energy in the modeled currents is consistent with that observed. Values comparable to the time scales of storm events (0.2-1 day^{-1}) seem to yield reasonable results.

The turbulent quantities q^2 and $q^2 \ell$ in equation (3) and equation (4) are used to derive the mixing coefficients for momentum (K_M), turbulence (K_q), and tracers (K_H) using the Mellor-Yamada 2.5 turbulence closure scheme (Mellor & Yamada, 1982). Terms on the right hand side of these equations represent the transport of turbulence, generation of turbulence via shear, and suppression of turbulence via stratification and dissipation. B_1, E_1, E_2, and E_3 are constants equal to 16.6, 1.8, 1.33 and 1.0, respectively. g is the acceleration due to gravity, and W is a "wall proximity function" which limits the eddy length scale near boundaries. Further details of the turbulence closure and boundary conditions for the turbulent quantities are described below.

The temperature and salinity equations are given by:

$$\frac{\partial T}{\partial t} = \frac{\partial}{\partial z} K_V \frac{\partial T}{\partial z} + ss \tag{5}$$

$$\frac{\partial S}{\partial t} = \frac{\partial}{\partial z} K_V \frac{\partial S}{\partial z} + ss \tag{6}$$

In the equation (5) and equation (6), ss represents a variety of source and sink terms for temperature and salinity. Temperature changes are driven by incident radiation and sensible, latent, and longwave heat fluxes. A net heat transport via advection can also be specified. Salinity changes are presently driven via relaxation to specified values. These sources and sinks are described in detail in the sections that follow. T and S are translated to a density using a routine from Phil Morgan's CSIRO seawater toolbox (UNESCO 1983 polynomial). Water is modeled as incompressible for this calculation.

2.1.1 Wind forcing

Wind input is provided as u- and v-components of speed in m/s, and translated to wind stresses using Large & Pond (1981). The stress (N m^{-2}) is calculated as

$$\tau_x = \rho_{air} C_d |W_{10}| U_{10} \tag{7}$$

$$\tau_y = \rho_{air} C_d |W_{10}| V_{10} \tag{8}$$

where W_{10} is the wind speed at 10m, C_d is a dimensionless drag coefficient, and ρ_{air} is the air density (which is assumed to be 1.25 kg m^{-3}). W_{10} is calculated from the measured wind speed assuming a logarithmic velocity profile. C_d is an empirical function of the wind speed:

$$
C_d = \begin{cases} 1.2 \times 10^{-3} & W_{10} < 11 \text{ ms}^{-1} \\ 1.0 \times 10^{-3}(0.49 + 0.065W_{10}) & W_{10} \geq 11 \text{ ms}^{-1} \end{cases} \tag{9}
$$

The `wstress.m` routine from Rich Signell's Matlab toolbox is used for this calculation.

2.1.2 Bottom stresses

The Princeton Ocean Model Formulation from of Mellor (2004) is used to calculate the bottom stress:

$$
\tau_{x,b} = \rho C_{bot} \left(U^2 + V^2 \right)^{1/2} U \tag{10}
$$

$$
\tau_{y,b} = \rho C_{bot} \left(U^2 + V^2 \right)^{1/2} V \tag{11}
$$

where C_{bot} is a bottom drag coefficient calculated as:

$$
C_{bot} = \max \left(\frac{\kappa^2}{\ln\left(\frac{0.5dz}{z_{ob}} \right)}, 0.0025 \right) \tag{12}
$$

where κ is Von-Karman's constant (0.4, dimensionless), dz is the width of the bottom grid cell (m), and z_{ob} is a bottom roughness coefficient. The basic form of this relationship comes from a logarithmic boundary layer solution. z_{ob} is given a value of 0.01 by default, which is indicative of a rather smooth boundary. The lower C_{bot} limit comes into play only when dz resolution is very large relative to the roughness length scale. It was inserted to be consistent with the POM formulation, but can be avoided as long as dz/z_{ob} ~ 5000.

2.1.3 The turbulence closure sub-model

Vertical mixing is determined using the Mellor-Yamada 2.5 turbulence closure scheme (Mellor & Yamada, 1982) with adjustments and simplifications described in Galperin et al. (1988) and Mellor (2004). Mixing coefficients are derived from the turbulent quantities q^2 and ℓ which are tracked prognostically via equation (3) and equation (4). The boundary condition for q^2 accounts for waves and is taken from equation (10) of Mellor & Blumberg (2004):

$$
q^2(0) = (15.8\alpha_{CB})^{2/3} u_\tau^2(z = 0) \tag{13}
$$

where u_τ is the surface "friction velocity" driven by the wind ($\sqrt{\tau_{wind}/\rho_w}$, where ρ_w is the surface water density). Mellor & Blumberg (2004) suggest using $\alpha_{CB} = 100$. A minimum value of 0.0001 is applied, which corresponds to a wind ~1 m/s. The bottom boundary condition for q^2 is calculated from equation 16a of Mellor (2004):

$$
q^2(z = z_{bot}) = B_1^{2/3} u_\tau^2(z = z_{bot}) \tag{14}
$$

5

where $u_\tau(z = z_{bot})$ is the bottom friction velocity. The length scale ℓ at the surface is from equations 5a and 6a of Mellor & Blumberg (2004):

$$\ell(z = 0) = \kappa z_w = \kappa \beta \frac{u_{tau}^2(z = 0)}{g} \tag{15}$$

where β is 2.0×10^5 and κ is von Karman's constant (0.41). The non-zero length scale at the ocean surface reflects the surface wave roughness. A minimum z_w value of 0.02 was imposed. This corresponds to waves generated by a wind of 1 m s^{-1} and is meant to mimic the persistence of some wave energy through calm periods.

ℓ at the bottom boundary was set to 0.

The wall proximity function W limits ℓ near the boundaries by enhancing the dissipation. The formulation used is:

$$1 + E_2 \left(\frac{\ell}{\kappa L} \right)^2 \tag{16}$$

where E_2 is a constant (1.33) and L is the distance from the surface or the bottom of the water column:

$$L = \frac{1}{|z|} + \frac{1}{|z_{bot} - z|} \tag{17}$$

Various wall proximity functions can be found in the literature and model codes. This one is very similar to those found in various versions of the Princeton Ocean Model and was taken from Williams (2006).

ℓ is limited in stably stratified flows in accordance with eqs. (22), (26) and (30) of Galperin et al. (1988). This is done using the quantity:

$$G_H = \frac{\ell^2 g}{q^2 \rho_0} \frac{\partial \rho}{\partial z} \tag{18}$$

which is the ratio of potential ($\frac{g}{\rho_0} \frac{\partial \rho}{\partial z}$) to kinetic energy ($\frac{\ell^2}{q^2}$). Since $\frac{\partial \rho}{\partial z}$ is negative in stable water columns (i.e. z=0 at the water surface and becomes more negative with depth), G_H is negative in stable water columns. Galperin et al. (1988) found it necessary to limit ℓ in highly stable flows such that stayed below 0.28. Minimum values of 1e-9 are imposed on both q^2 and $q^2\ell$ in accordance with the POM2K code.

The diffusivities are calculated from q^2 and following Mellor & Yamada (1982) and Galperin et al. (1988):

$$K_M = q\ell S_M \tag{19}$$

$$K_H = q\ell S_H \tag{20}$$

$$K_q = 0.41 q\ell S_H \tag{21}$$

The factors S_M and S_H all depend on G_H according to:

$$S_H = \frac{A_2 \left(1 - 6\frac{A_1}{B_1}\right)}{1 - (3A_2 B_2 - 18 A_1 A_2) G_H} \sim \frac{0.49}{1 - 34.68 G_H} \tag{22}$$

A_1, A_2, B_1, and B_2 are empirical constants that are 0.92, 0.74, 16.6, and 10.1, respectively. Because $S_H \to \infty$ for G_H values approaching 0.028 (unstable, high energy conditions), values of G_H are capped at 0.028. $S_H \to 0$ as $G_H \to -\infty$ (highly stable or low energy conditions). For S_M:

$$S_M = \frac{A_1 \left(1 - 3C_1 - 6\frac{A_1}{B_1}\right) + S_H \left[\left(18 A_1^2 + 9 A_1 A_2\right) G_H\right]}{1 - 9 A_1 A_2 G_H} \sim \frac{0.39 + 21.36 S_H G_H}{1 - 6.1 G_H} \tag{23}$$

where C_1 is 0.08. This factor also approaches 0 as $G_H \to -\infty$.

2.1.4 Heat forcing

The heat forcing input calls for the incident flux, air temperature, and the dew point temperature. Sensible, latent, and longwave fluxes are calculated using various bulk formulae described below. This has the advantages of relying on commonly measured quantities and allowing feedbacks between observed atmosphere conditions and the calculated ocean temperature. Such feedbacks reduce the probability of developing large, persistent biases over long model runs.

The incident irradiance (Q_i) is entered in watts m^{-2} and the model assumes that data represents energy over the wavelength range measured by most pyranometers (300-5000 nanometers). This is adjusted downward according to the albedo specified in the input data. 45% of the Q_i is assumed to be from the photosynthetically available range (350-700 nm, Baker & Frouin, 1987). By default, this energy is assumed to have an attenuation coefficient of 0.15 m^{-1}. The remaining fraction is attributed to infrared wavelengths and is absorbed rapidly (1.67 m^{-1}). Self-shading by phytoplankton is applied within the primary production calculations in the ecosystem model but does not feed back to the physical state variables.

The Friehe & Schmitt (1976) formulae are used to estimate the sensible heat flux (Q_s, watts m^{-2}):

$$Q_s = \rho_{air} C_p \overline{\omega\theta} \tag{24}$$

where ρ_{air} is the air density (assumed to be ~1.2 kg m^{-2}), C_p is the specific heat capacity of air (1000 J kg^{-1} K^{-1}), and $\overline{\omega\theta}$ is the mean vertical velocity-temperature covariance (m K s^{-1}). This latter term is estimated as a function of wind speed at 10m (W_{10}) and the sea-air temperature difference ($\Delta T = T_{ocean} - T_{air}$):

$$\overline{\omega\theta} = \begin{cases} 0.002 + (0.97 \times 10^{-3})W_{10}\Delta T & 0 < W_{10}\Delta T < 25 \text{ (unstable)} \\ (1.46 \times 10^{-3})W_{10}\Delta T & W_{10}\Delta T \geq 25 \text{ (highly unstable)} \\ 0.0026 + (0.86 \times 10^{-3})W_{10}\Delta T & W_{10}\Delta T \leq 0 \text{ (stable)} \end{cases} \tag{25}$$

The sensible heat goes exclusively into the top grid cell.

The formulae of Friehe & Schmitt (1976) are also used to estimate the latent heat flux (Q_L, watts m^{-2}):

$$Q_L = L_e \overline{wq} \tag{26}$$

where $\overline{wq}$ is the mean vertical velocity-water vapor density covariance (m s^{-1} g m^{-3}) and L_e is the latent heat of evaporation (2250 J g^{-1}). This is estimated with the formula:

$$Q_L = L_e(1.32 \times 10^{-3})W_{10}(q_s - q_a) \tag{27}$$

where q_s is the water vapor density (g m^{-3}) at the sea surface, and q_a is the water vapor density (g m^{-3}) at a reference height above the ocean surface (~10m). q_s is calculated as the saturation humidity at the sea surface temperature (following the approach used in the Princeton Ocean Model). q_a is determined from the measure dew point temperature in the model forcing. The approximation $e_s = Ae^{\beta T}$ is used to calculate the saturated vapor pressure at temperature T for these calculations, where $A = 611$ Pa and $\beta = 0.067$ °C^{-1}. This was taken from Marshall & Plumb (2008; p. 6) and gives of the saturated vapor pressure at typical atmospheric conditions.

The longwave flux (Q_{LW}) is calculated using the Efimova formula as reported by Simpson & Paulson (1979). This calculates the clear-sky longwave radiation flux as:

$$Q_{LW,clear} = \varepsilon \sigma T_{srf}^4 \left(0.254 - 0.00495 e_a\right) \tag{28}$$

where ε is the emissivity of the surface (0.97), σ is the Stefan-Boltzman constant (5.67e-8 W m^{2}K^{-4}), T_{srf} is the surface ocean temperature (K), and e_a is the atmospheric vapor pressure (in mb = 100 Pascals). The clear sky longwave radiation loss is adjusted downward by a cloud correction factor of the form:

$$Q_{LW} = Q_{LW,clear}(1 - 0.8C) \tag{29}$$

where C is the ratio of the observed incident radiation (Q_i) over 24 hours and the clear-sky value estimated using the Smithsonian formulas as reported in Reed (1977). These calculations are done during the model initialization. The clear-sky irradiance is calculated as a function of latitude and time of year. As of the writing of this description, only formulae good for latitudes from 20°S-60°N are included. The details can be found in the routine `clearsky.m`.

A net heat flux due to advection (Q_{adv}) can also be considered. This heat is added as a source/sink term over a depth scale (δ) following the approach of Umoh & Thompson (1994):

$$Q_{adv}(z) = Q_{adv,o} \frac{\exp\left(\frac{z}{\delta}\right)}{\delta \left(1 - \exp\left(-\frac{h}{\delta}\right)\right)} \tag{30}$$

This assumed that the majority of the depth-integrated heat flux ($Q_{adv,o}$) is distributed over the depth scale δ, which is effectively an e-folding scale for the heat transport. h in the above expression it the total depth of the water column.

2.2 Input variables for the Eastern Subarctic Gyre

For the most recent set of simulations (the volcano study), we required realistic interannual variability, so we used a combination of reanalysis products for our input forcing. For atmospheric forcing (wind speed and direction, solar radiation, air temperature, and dew point temperature), we used the ECMWF ERA-Interim dataset. Water column properties, including temperature and salinity profiles, derived from ocean state estimates from ECCO Version 4 Release 1.
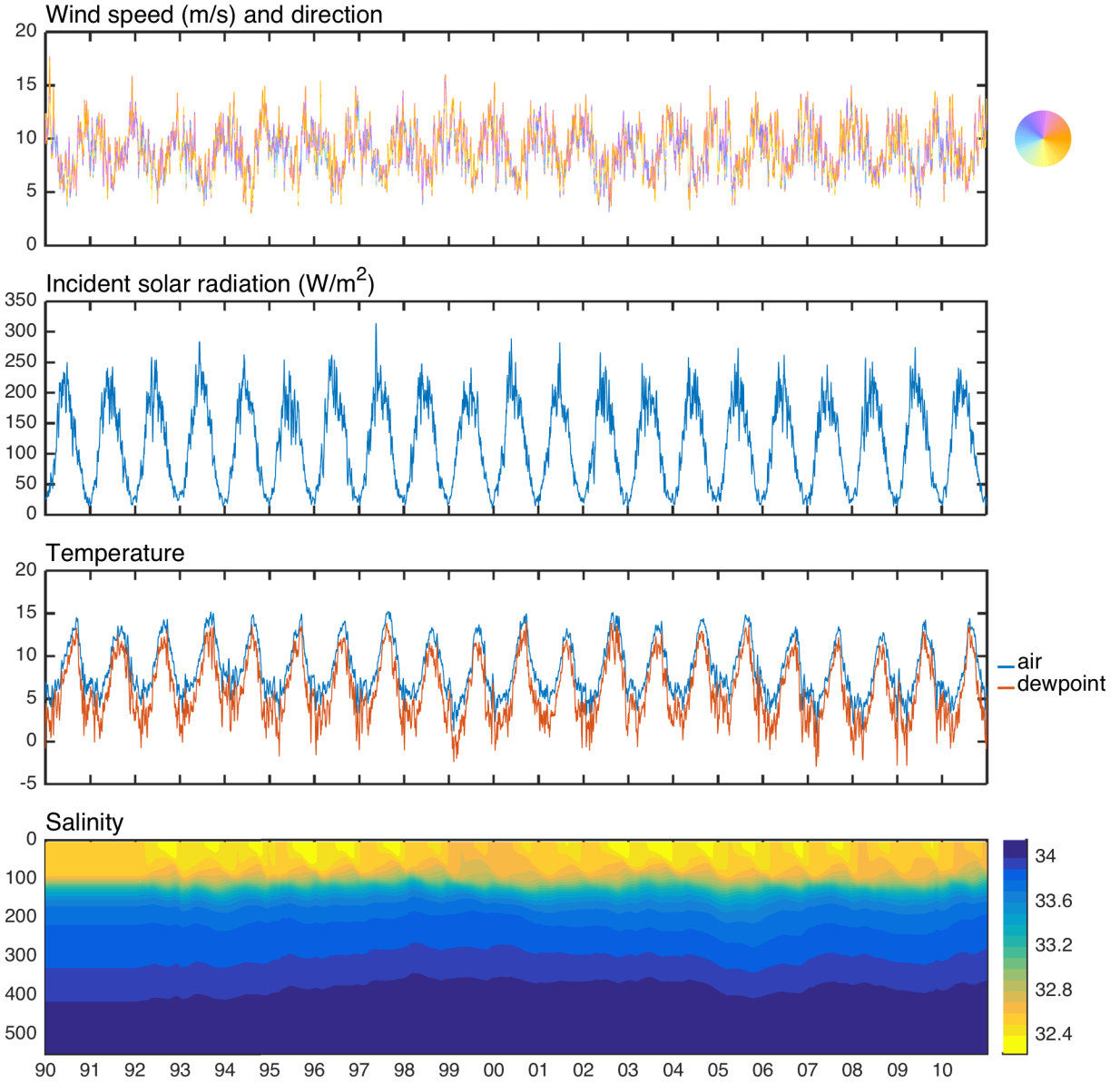
Figure 1: Input datasets used to force the physical model. Atmospheric forcing data is shown with a 30-day moving average applied for clarity.

3 The biological module

3.1 Model framework and equations

The water column ecosystem model consists of 8 non-living state variables (particulate and dissolved nutrients) and 3 classes of living state variables (phytoplankton, zooplankton, and nekton), coupled together by three sets of ordinary differential equations, one for each of the three nutrients included in the model.

The designation of living functional groups as either planktonic or nektonic reflects both their relationship to the physical model and their interactions with other functional groups. The planktonic label refers to any group whose movement is strongly influenced by the movement of the water in which they reside; these groups are resolved with depth, can feed only on functional groups occupying the same depth layer as themselves, and are subject to mixing via advection and diffusion in the same manner as all physical tracers. The nektonic label refers to all other living organisms, including those that do not live in the water but feed on marine organisms (such as birds); these groups are not subject to any mixing, and they feed on the integrated sum over depth of their prey groups.

Physical and biological ODEs are solved consecutively for the biological variables. At each model time step, the biological state variables are first mixed, where applicable, following the same formulation as equation (??), with the source minus sink term representing any additional vertical movement. In most of my simulations, this term is used to apply sinking velocities to the particulate state variables (PON, $Opal$, and $POFe$), and to prescribe vertical migration behavior to the copepod group. Following this, the set of ODE equations describing the exchange of biomass between the biological state variables is solved using a fourth-order fixed-step solver with a 3-hour time step.

The biological ODEs are based on the addition of several processes: gross primary production, extracellular excretion, respiration, grazing, predation, excretion, egestion, non-predatory mortality, decomposition and remineralization, iron uptake, and iron scavenging (Figure 2). The following sections describe each of these processes in detail.

A note on subscripts, which are plentiful in this documentation: subscripts indicate the index of a functional group to which a given process variable or parameter pertains. I typically use i as this index, and expand to j and k when I need to represent more than one functional group in a single equation. Where variables are related to fluxes between groups, they are denoted by two subscripts (e.g. x_{ij}), with the source group index followed by the sink group index. For clarity I often separate multiple subscripts from each other with commas (e.g. x_{NH_4,NO_3} represents a parameter relating to a flux from the NH_4 state variable to the NO_3 variable); commas also separate parameter-name subscripts from functional group subscripts (e.g. $V_{max,PS}$ is the V_{max} growth rate parameter associated with the PS state variable).

The values of the various biological state variables are referred to as B_i in all the equations below; depending on the particular state variable, these can be thought of as either biomass values or nutrient concentrations. All phytoplankton groups are represented by three state variables: phytoplankton nitrogen (B_i), phytoplankton silica ($B_{Si,i}$), and phytoplankton iron ($B_{Fe,i}$), while zooplankton and nekton groups consist of only nitrogen state variables.

3.1.1 Gross Primary Production (Gpp)

Gross primary production fluxes flow from the NO_3 and NH_4 variables to each phytoplankton group, following Kishi et al. (2007), with the addition of iron limitation. The uptake of nitrogen is described by:

$$Gpp_i = V_{max,i} \exp(K_{gpp,i}T) \cdot L_{nut,i} \cdot L_{light,i} \cdot B_i \tag{31}$$
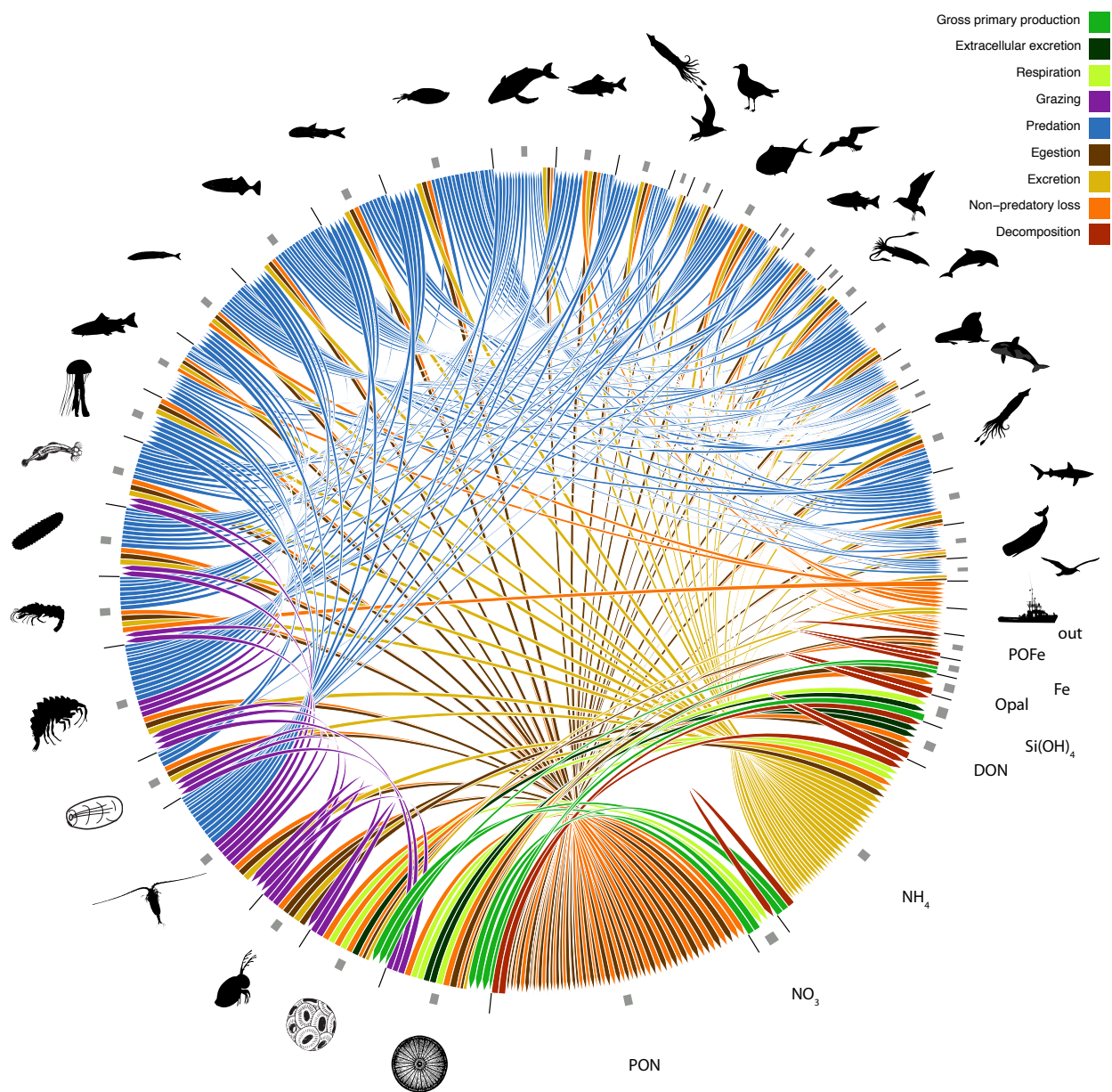
Figure 2: Ecosystem processes linking the various biological state variables, using the Eastern Subarctic food web model.

where B_i is the nitrogen-based biomass of group i, resolved with depth. See Table 2 and Table 10 for parameter values.

3.1.2 Respiration (Res)

Respiration applies to all phytoplankton groups, and flows from the phytoplankton to the NO_3 and NH_4 groups following the same f-ratio as uptake via primary production:

$$Res_i = Res_{0i} \exp(K_{res,i} T) B_i \tag{32}$$

See Table 4 for parameter values.

3.1.3 Extracellular excretion (Ex)

Extracellular excretion applies to all phytoplankton groups, and flows from the phytoplankton to the DON group. Following Kishi et al. (2007), extracellular excretion is proportional to the flux due to gross primary production:

$$Ex_i = \gamma_i \cdot Gpp_i \tag{33}$$

See Table 5 for parameter values.

3.1.4 Consumption (Con)

Predator/prey interactions between functional groups follow the Aydin version of the foraging arena functional response. The exact form of the functional response varies based on whether the predator and prey groups are planktonic or nektonic. For interactions between two planktonic groups, the flux (referred to as grazing in Figure 2) is resolved with depth for both the predator and prey group, and the uptake rates are temperature-dependent:

$$Con_{ij} = \frac{Q'_{ij}}{\exp(K_{Gra,i} \cdot T_{avg})} \exp(K_{Gra,i} \cdot T) \left(\frac{X_{ij} \cdot \frac{B_j}{B'_j}}{X_{ij} - 1 + \frac{B_j}{B'_j}} \right) \left(\frac{D_{ij} \cdot \left(\frac{B_i}{B'_i} \right)^{\theta_{ij}}}{D_{ij} - 1 + \left(\frac{B_i}{B'_i} \right)^{\theta_{ij}}} \right) \tag{34}$$

where here, the subscripts i and j represent the prey and predator groups, respectively. The biomass and consumption rate parameters are derived from the Ecopath mass balance: $Q' = \frac{Q^*}{MLD}$ and $B' = \frac{B^*}{MLD}$, where Q^* and B^* are the per-area mass-balanced quantities returned directly from Ecopath. The parameters MLD and T_{avg} describe the yearly averaged mixed layer depth and mixed layer temperature, respectively, as simulated by the one-dimensional physical model.

For interactions between two nektonic groups, the functional response follows the same form, but in units of biomass integrated over depth (termed predation in Figure 2). For shorthand, $Bint$ is used for depth-integrated biomass. Nektonic consumption does not vary with temperature.

$$Con_{ij} = Q^*_{ij} \left(\frac{X_{ij} \cdot \frac{Bint_j}{B^*_j}}{X_{ij} - 1 + \frac{Bint_j}{B^*_j}} \right) \left(\frac{D_{ij} \cdot \left(\frac{Bint_i}{B^*_i} \right)^{\theta_{ij}}}{D_{ij} - 1 + \left(\frac{Bint_i}{B^*_i} \right)^{\theta_{ij}}} \right) \tag{35}$$

When a nektonic group preys upon a planktonic group, the total flux is calculated in depth-integrated units. However, the loss on the plankton side is resolved with depth and distributed proportionally to the prey biomass at each depth (equation (36)), while the flow to the predator remains in depth-integrated units (equation (37)):

$$Con_{ij} = Q^*_{ij} \left(\frac{X_{ij} \cdot \frac{Bint_j}{B^*_j}}{X_{ij} - 1 + \frac{Bint_j}{B^*_j}} \right) \left(\frac{D_{ij} \cdot \left(\frac{\int_0^{z_{max}} B_i dz}{B^*_i} \right)^{\theta_{ij}}}{D_{ij} - 1 + \left(\frac{\int_0^{z_{max}} B_i dz}{B^*_i} \right)^{\theta_{ij}}} \right) \cdot \frac{1}{\Delta z} \cdot \frac{B_i \Delta z}{\int_0^{z_{max}} B_i dz} \tag{36}$$

$$ConI_{ij} = Q^*_{ij} \left(\frac{X_{ij} \cdot \frac{Bint_j}{B^*_j}}{X_{ij} - 1 + \frac{Bint_j}{B^*_j}} \right) \left(\frac{D_{ij} \cdot \left(\frac{Bint_i}{B^*_i} \right)^{\theta_{ij}}}{D_{ij} - 1 + \left(\frac{Bint_i}{B^*_i} \right)^{\theta_{ij}}} \right) \tag{37}$$

In the most recent version of the model code, an additional parameter is assigned to each predator, indicating prey visibility (as a fraction from 0-1) versus depth. It is used to adjust B_i and $Bint_i$ values to each predator based on the foraging/hunting behavior of the predator. This allows us to, for example, limit nektonic predation to only the upper portion of the water column for pelagic species.

See Table 6, Table 13, and Table 14 for parameter values.

3.1.5 Excretion (Exc) and egestion (Ege)

Egestion and excretion are proportional to the total consumption of prey by a predator. Egestion flows from the predator to the PON group. Excretion flows from the predator group to the NH_4 group. All excretion and egestion by nektonic groups is assumed to take place in the surface layer:

$$Ege_i = GS_i \cdot \left(\sum_{k=plank} Con_{ki} + \frac{\sum_{\ell=nek} ConI_{\ell i}}{\Delta z_1} \right) \qquad z = 1 \tag{38}$$

$$Ege_i = GS_i \cdot \sum_k Con_{ki} \qquad z \neq 1 \tag{39}$$

$$Exc_i = (1 - GE_i - GS_i) \cdot \left(\sum_{k=plank} Con_{ki} + \frac{\sum_{\ell=nek} ConI_{\ell i}}{\Delta z_1} \right) \qquad z = 1 \tag{40}$$

$$Exc_i = (1 - GE_i - GS_i) \cdot \sum_k Con_{ki} \qquad z \neq 1 \tag{41}$$

See Table 13 for parameter values.

3.1.6 Non-predatory mortality (Mor)

The non-predatory loss process is used to represent the net effect of a diversity of loss processes, including natural mortality (i.e. death due to old age), loss to disease and viruses, unresolved intra-group mortality (such as egg cannibalism and predation on juveniles of similar species), aggregation and sinking out of the modeled system (primarily of large phytoplankton), and metabolic costs. It flows from each living functional group to the PON group, and is allowed to vary in functional form between groups, based on the exponent parameter c_i. A value of $c_i = 1$ leads to linear mortality, while $c_i = 2$ indicates a quadratic loss term. See Kearney et al. (2013) for a detailed sensitivity study related to this exponent term. For planktonic groups, the non-predatory flux is in units of mass per volume:

$$Mor_i = \left(\frac{M_{0i}}{B_i'^{(c_i-1)}} \right) \cdot B_i^{c_i} \tag{42}$$

while for nektonic groups it is in units of mass per area:

$$MorI_i = \left(\frac{M_{0i}}{B_i^{*(c_i-1)}} \right) \cdot Bint_i^{c_i} \tag{43}$$

As with egestion and excretion by nektonic groups, non-predatory mortality of nektonic groups is assumed to occur in the surface layer, such that in the surface layer,

$$Mor_i = \frac{MorI_i}{\Delta z_1} \tag{44}$$

when $i =$ nekton.

See Table 9 and Table 13 for parameters.

3.1.7 Proportional-to-nitrogen fluxes of silica and iron

The majority of fluxes between iron- and silica-based state variables occur in proportion to nitrogenous fluxes. Silica fluxes due to gross primary production (Gpp), extracellular excretion (Ex), and respiration (Res) between phytoplankton groups and $SiOH_4$ occur in a constant proportion to the respective fluxes in nitrogen between phytoplankton groups and all dissolved nitrogen pools (NO_3, NH_4, and DON). Similarly, fluxes due to non-predatory mortality (Mor) from phytoplankton groups to the PON group are accompanied by proportional fluxes of silica from the large phytoplankton to particulate opal group. Silica is assumed to be completely egested by phytoplankton grazers, so the proportional flux due to predator consumption (Con) of phytoplankton silica is routed entirely to the particulate opal group, rather than being split between predator, egestion, and excretion as is the case for nitrogenous consumption.

Iron fluxes between the two phytoplankton groups and the dissolved and particulate iron groups also occur proportionally to nitrogen fluxes, though the ratio between the two elements varies over time (see Section 3.1.9).

14

3.1.8   Decomposition (Dec)

Decomposition fluxes follow the model of Kishi et al. (2007), with a decay rate related to temperature:

$$Dec_{ij} = V_{Dec,ij} \exp(K_{Dec,ij}T) \cdot B_i \tag{45}$$

where the subscripts i and j represent the source and sink groups, respectively, and B_i the concentration of the source group.

See Table 8 for parameters.

3.1.9   Iron uptake (Qup)

This iron model is based closely on one developed for the Carbon, Ocean Biogeochemistry and Lower Trophics (COBALT) marine ecosystem model (Stock et al., in press), with a few adjustments to parameter values in order to tune the dynamics to a one-dimensional water column.

Iron uptake, flowing from the Fe group to each phytoplankton group, is based on an internal cell quota of the phytoplankton, accounting for both requirements and additional luxury uptake. Iron's contribution to overall nutrient limitation, which regulates the uptake of macronutrients, is termed iron deficiency ($D_{Fe,i}$) and is calculated based on the internal ratio of iron to nitrogen. However, uptake of iron is not proportional to uptake of nitrogen, but instead based on a separate limitation term ($L_{Fe,i}$), allowing phytoplankton to increase their internal Fe:N ratios to a preset limit:

$$Qup_i = \begin{cases} V_{max,i} \exp(K_{gpp,i}T) \cdot B_{Fe,i} \cdot L_{Fe,i} \cdot \mu_{Fe:N,i}, & \text{if } R_{Fe:N,i} < R_{Fe:Nmax,i} \\ 0, & \text{otherwise} \end{cases} \tag{46}$$

Iron is not tracked beyond the level of phytoplankton, but upon loss to predation is recycled to the dissolved and particulate iron state variables proportionate to the nitrogenous excretion and egestion fluxes of their predators.

See Table 3 for parameters.

3.1.10   Iron scavenging (Ads)

Scavenging of dissolved iron onto particles (Fe to $POFe$) follows a single ligand model, where only non-ligand-bound iron is available for adsorption onto particles. Light is assumed to greatly reduce the effectiveness of ligand binding through the production of oxygen free radicals (Fan, 2008). This impact is assumed to decay at light levels below 10 W m^{-2} in a manner consistent with the observed decline of hydrogen peroxide in the water column (Yuan & Shiller, 2001). The free unbound iron, Fe_{free}, is calculated via:

$$K_{Lig} \cdot Fe_{free}^2 + (1 + K_{Lig} \cdot (Lig_{bkg} - Fe)) \cdot Fe_{free} - B_{Fe} = 0 \tag{47}$$

Adsorption onto particles is directly proportional to this free iron. Iron scavenging rates have been observed to be lower above dissolved iron concentrations of 0.6 nM, possibly due to less complexation with ligands at these concentrations(Johnson et al., 1997), so the final scavenging equations allow for this:

$$Ads = \begin{cases} \alpha_{scav} \cdot Fe_{free} & Fe_{free} \leq 0.6 \\ 0.08 \cdot (Fe_{free} - 0.6) \cdot \alpha_{scav} \cdot Fe_{free} & Fe_{free} > 0.6 \end{cases} \tag{48}$$

Finally, a fraction of particulate iron is remineralized to the dissolved iron pool, proportional to remineralization of particulate nitrogen to ammonium.

$$Dec_{POFe,Fe} = Dec_{PON,NH_4} \cdot \frac{B_{PON}}{B_{POFe}} \cdot r_{eff} \tag{49}$$

See Table 3 for parameters.

3.1.11 Rerouting of fluxes

By default, the flux processes move biomass from specific source and sink groups as described in the sections above. But they can also be redirected in order to tune the model a bit to specific behaviors of individual functional groups.

In the Eastern Subarctic Gyre ecosystem model, the following rerouting adjustments were made:

1. Small phytoplankton non-predatory mortality: 25% is redirected to DON and 25% is redirected to NH_4. The small size of this group means that their loss contributes little to the heavy, sinking particles of the PON group.

2. Microzooplankton egestion: 25% is redirected to DON and 25% is redirected to NH_4. They prey on small phytoplankton, and again, this flux behaves more like dissolved material than sinking particulates.

3. Non-predatory mortality of birds, mammals, and sharks (albatross, sperm whales, toothed whales, elephant seals, seals/dolphins, fulmars, skuas/jaegers, puffins/shearwaters/storm petrels, kittiwakes, sharks): 90% redirected out of the system. Loss of these groups typically occur outside of the modeled system, either out of the water or sinking quickly to deep water, and therefore little of their biomass is recycled to the nutrient pools of the modeled system.

4. Non-predatory mortality of fisheries target species (pomfret, chum salmon, chinook/coho/steelhead, sockeye/pink, saury, sergestid shrimp): 90% is redirected to fishing loss. Our initial Ecopath model does not explicitly resolve fisheries loss, instead including this loss with other non-predatory losses. This redirection removes these losses from the flux back into the nutrient pools, and allows us to quantify a rough estimate of fisheries landings.

3.2 Input data for the Eastern Subarctic Gyre

3.2.1 The Ecopath Model

The coupled model relies on the Ecopath mass-balance modeling concept (Christensen & Walters, 2004) to calculate a large number of the ecosystem parameters related to upper trophic level processes: specifically, grazing, predation, excretion and egestion, and non-predatory mortality. The majority of the Ecopath data used to construct our food web model came from a previously-published model, developed through a series of PICES-sponsored workshops to look at similarities and differences between the eastern and western subarctic gyres of the north Pacific Ocean (Aydin et al., 2003); I refer to this model as the Aydin-48 model because

it included 48 functional groups. A few modifications were made to this Ecopath model in preparation for using it in this framework.

The first modification made was to eliminate the bacteria functional group from the Aydin-48 model. In the original model, this functional group was included as a prey item for microzooplankton, "preying" itself on the two detrital functional groups. However, in their time-dynamic simulations, Aydin et al. (2003) found that their results were highly sensitive to this representation of the microbial loop, and it led to some lower trophic level dynamics that disagreed with accepted biogeochemical models from the region; they concluded that it was sufficient to assume that bacterial processes occurred within the detrital pools and removed the bacteria group from some of their later simulations. Because we intended to link the Ecopath-derived food web model directly to a biogeochemical model that already included parameterizations for the microbial loop, we decided to eliminate the bacteria group from the food web dynamics entirely, and we replaced the microzooplankton diet with one of 100% small phytoplankton.

Table 1 provides descriptions of the 47 functional groups that remained in the model, including the most common species classified under each functional group. Pertinent information regarding each group's lifecycle is also provided.

After examining the sources of zooplankton data for the Aydin-48 model, we made several adjustments to the data for those groups. Aydin et al. (2003) resolved the zooplankton community into eleven different functional groups: microzooplankton, copepods, euphausiids, pteropods, amphipods, sergestidae (shrimp), chaetognaths, salps, ptenohores, large jellyfish, and a miscellaneous group (mainly larvaceans and polychaetes). Much of the data for these groups was derived from a simulation of the NEMURO biogeochemical model. We found several points of disagreement with the assumptions used to translate the NEMURO output data into Ecopath input data.

First, the version of NEMURO used by Aydin et al. (2003) was an early realization of that model (Eslinger et al., 2000; Megrey et al., 2000). For this study, we developed our own biogeochemical model, based very closely on NEMURO but with the addition of iron dynamics, and substituted the values from a simulation of our model in place of those detailed in the Aydin et al. (2003) report.

Second, Aydin et al. (2003) interpreted NEMURO's predatory zooplankton group (ZP) as representing only non-gelatinous omnivores, i.e. euphausiids, pteropods, and amphipods. They gathered data for the gelatinous zooplankton groups (large jellyfish, chaetognaths, salps, and ctenophores) from other sources, and estimated the population of the carnivorous shrimp and miscellaneous groups each as 10% of the ZP value. Overall, this led to a community with a very large mesozooplankton community, more than twice that of the copepod population, despite the fact that copepods should be the dominant mesozooplankton genera at this location (Goldblatt et al., 1999; Harrison et al., 2004). While NEMURO's ZP state variable does have an omnivorous diet, in our opinion it was intended to represent all unresolved predators of the two smaller zooplankton state variables (which correspond to the microzooplankton and copepod populations); in this Ecopath model, this includes not only the nine remaining zooplankton groups but also all other non-planktonic groups. Based on descriptions of the mesozooplankton community in the subarctic gyre (Goldblatt et al., 1999), we decided to distribute 50% of the ZP biomass across the omnivorous, non-gelatinous zooplankton groups (euphausiids, pteropods, and amphipods), 40% across the omnivorous, gelatinous groups (salps and ctenophores), and the remaining 10% across the carnivorous groups (shrimp, ctenophores, and miscellaneous).

Another modification we made to the NEMURO-derived zooplankton biomass data in the Aydin et al. (2003) report involved the conversion of units between NEMURO, which tracks state variables through their nitrogen content, and Ecopath, which uses total wet weight. While Aydin et al. (2003) detailed the assumptions used to convert the NEMURO data from mmol N m^{-2} to g C m^{-2}, including elemental ratios and mixed layer depth values, no explanation was given for the 0.01 g C/g wet weight conversion factor that was then used to calculate wet weight of both phyto- and zooplankton groups. While this order of

magnitude estimate is common in conversions of fish wet weight to carbon content, it is much lower than most measurements for plankton. For example, crustacean zooplankton wet mass to carbon ratios range from 0.06-0.12 g wet mass/gC (Harris et al., 2000). We compromised with a conversion factor of 0.03 gC/g wet weight, which we applied throughout this study whenever converting between element-based and weight-based units.

The final adjustment we made to the Aydin-48 data concerned the growth efficiency value applied to the ctenophore group. The value of 0.03 used for this group appeared extremely low, even for a gelatinous group. Aydin et al. (2003) cited Pauly et al. (1996) as the source of this number. However, Pauly et al. (1996) derived their carnivorous jelly data from measurements of the cnidarian *Aglantha*, not a ctenophore, and even for this species they commented that the consumption rate they were using was "very high, perhaps excessively so." Measured growth efficiencies for ctenophores vary from less than 10% to 45% (Reeve et al., 1978; 1989); we settled on a value of 0.3, in line with that of the other zooplankton groups, in order to resolve Ecopath balance issues that arose as a result of the NEMURO-derived adjustments detailed above.

3.2.2 Food web clustering

In theory, the food web described in the previous section could be used to derive the necessary parameters to run a simulation of our model. However, for purely practical reasons (computation time, ease of analysis, ability to create plots that included all results and were still readable without a microscope, etc.), we preferred to decrease the number of functional groups to the smallest number that would still capture the processes of interest.

The simplification was performed via agglomerative hierarchical clustering. Our similarity metric for the clustering process included diet composition, using shared prey and predator groups as the main descriptive parameters, along with level of primary production and trophic level to maintain the basic trophic hierarchy in the clustered results (Figure 3). During initial development of the model, and in Kearney et al. (2012) and Kearney et al. (2013), I used the food web resulting from a similarity cutoff value of 1.5, which produces a 24-group model (23 living groups plus one detrital group). In more recent studies, I have used a lower cutoff value of 0.5, resulting in a 33-group model (32 living groups plus one detrital group).

The Ecopath input parameters for the 33-group model can be found in Table 11 and Table 12.

3.2.3 Ensemble generation

The construction of a typical Ecopath model involves the compilation of a large amount of population-related data, including biomass, production rates, consumption rates, diet fractions, growth efficiencies, and assimilation efficiencies for each functional group included in the model. These data typically come from a wide variety of sources, ranging from high-quality scientific surveys to fisheries landing data, empirical relationships, and other models. The uncertainty values on these numbers can be very high, up to or beyond an order of magnitude from the point estimates, and accurate measurement of these uncertainties is rare.

Although the inclusion of pedigree values, i.e. estimates of the quality of each parameter based on its underlying source, is relatively common when documenting Ecopath models, the uncertainty information is rarely incorporated into the predicted results deriving from these models (Christensen et al., 2005). However, the wide range of uncertainty associated with some input values means that often a single simulation based on the mean inputs does not capture the true range of possible outcomes; in some cases even the direction of change in one functional group as a result of a perturbation to a different group cannot be fully ascertained when accounting for the entire input range.
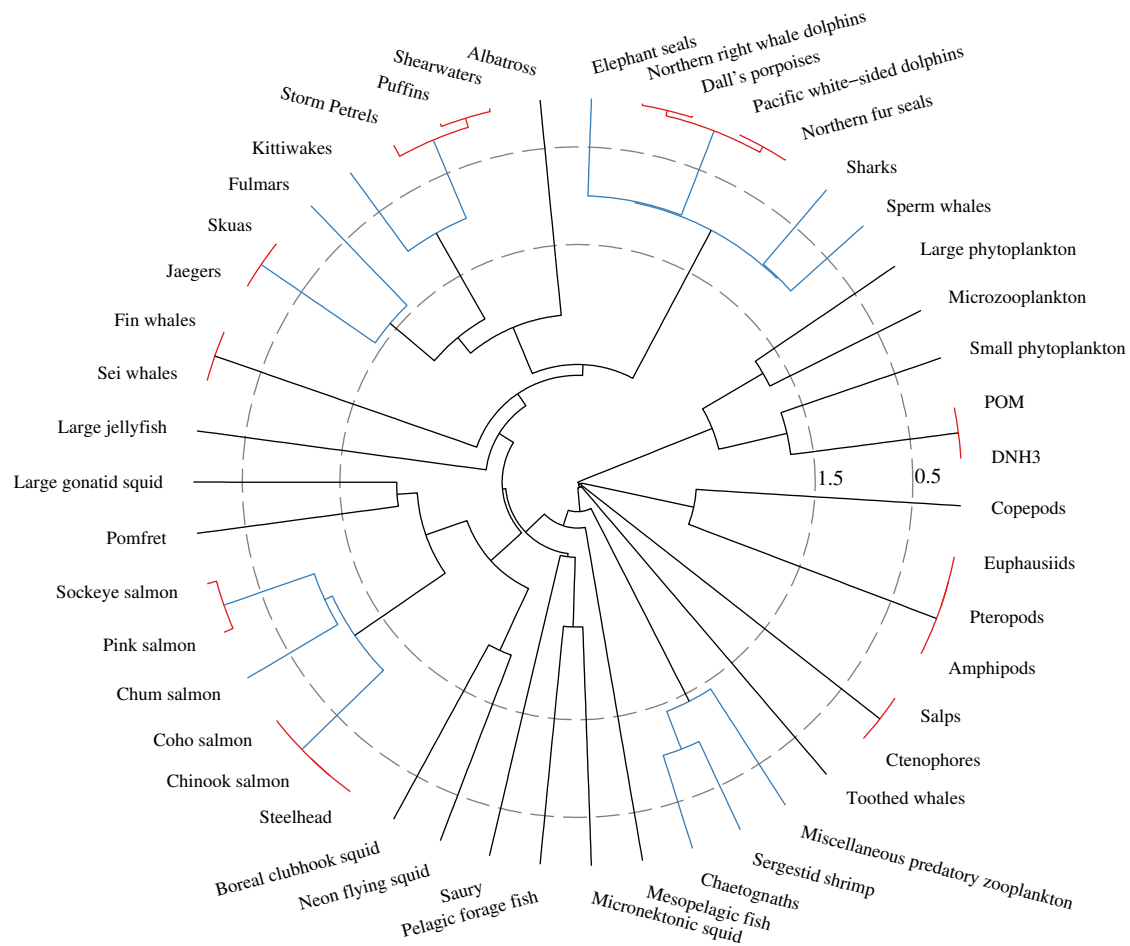
Figure 3: Dendrogram for food web clustering.

In previous work, when coupling an Ecopath-derived predator/prey model to a seasonally-varying biogeo-chemical model (Kearney et al., 2012; 2013), we found that small numerical differences in initial parameters could occasionally lead to outlier-type results. Rather than constantly readjusting the hundreds of parameters to find a single set of perfectly-tuned numbers that were both representative of the entire ecosystem and numerically well-behaved, we instead decided to use an ensemble of Ecopath models to derive our parameters and thereby encompass as much of the potential parameter space as possible. The process is as follows.

Step 1: For each user-input parameter in the model, choose n random values based on the prescribed probability density functions for each parameter. Currently, the code allows uncertainty to be applied to biomass (B_i), production per unit biomass ($\frac{P}{B}_i$), consumption per unit biomass ($\frac{Q}{B}_i$), ecotrophic efficiency (EE_i), growth efficiency (GE_i, or $\frac{P}{Q}_i$), and each component of the diet composition (DC_{ij}). Each parameter is assigned a lognormal distribution function with mean m and variance $\left(\frac{mp}{2}\right)^2$, where m is the initial point estimate for the parameter and p is the respective pedigree value; in terms of the lognormal probability density function

$$P(x, \mu, \sigma) = \frac{1}{x\sigma\sqrt{2\pi}} e^{-\frac{(\ln x - \mu)^2}{2\sigma^2}} \tag{50}$$

this leads to values of

$$\mu = \ln\left(\frac{m^2}{\sqrt{\left(\frac{mp}{2}\right)^2 + m^2}}\right) \tag{51}$$

$$\sigma = \sqrt{\ln\left(\frac{p^2}{4} + 1\right)} \tag{52}$$

The lognormal distribution was chosen so that the resulting values would always remain non-negative without the need for hard limits on the parameter ranges.

The remaining input variables, including assimilation efficiencies (GS_i), fishing loss due to landings and discards (Y_i), biomass accumulation (BA_i), and net migration due to immigration and emigration (E_i) remain as point estimates. In theory, the technique could easily be extended to include these parameters as well, but pedigree analyses tend to ignore these, likely for a variety of reasons (BA_i and E_i are typically non-zero for only a small number of groups in a model; Y_i only applies to fished species; GS_i is rarely modified from its default value of 0.2-0.3).

The sampling of parameter values from the defined distributions can be performed using any number of sampling schemes. Currently, the code provides two options: Monte Carlo sampling and latin hypercube sampling. Ecopath models typically include dozens of functional groups, connected to each other by dozens to hundreds of predator-prey linkages. This means that full multidimensional parameter space encompassed by the distribution functions of all input variables is nearly impossible to sample uniformly across the high number of dimensions, even with thousands of samples. The latin hypercube option chooses samples using a stratified design across each single parameter, such that the univariate parameter space is evenly sampled; it also incorporates a maximin criteria (Johnson et al., 1990) to maximize the minimum multidimensional distance between sample sets. While the sampling space of an Ecopath model will always be pretty sparsely sampled, the latin hypercube method allows for slightly better coverage of this multidimensional parameter space with a smaller number of ensemble members than simple Monte Carlo sampling.

Step 2: Substitute each set of parameters into the Ecopath model, and make the necessary adjustments to diet composition and multi-stanza group biomass and consumption rates. Some of the parameters in an
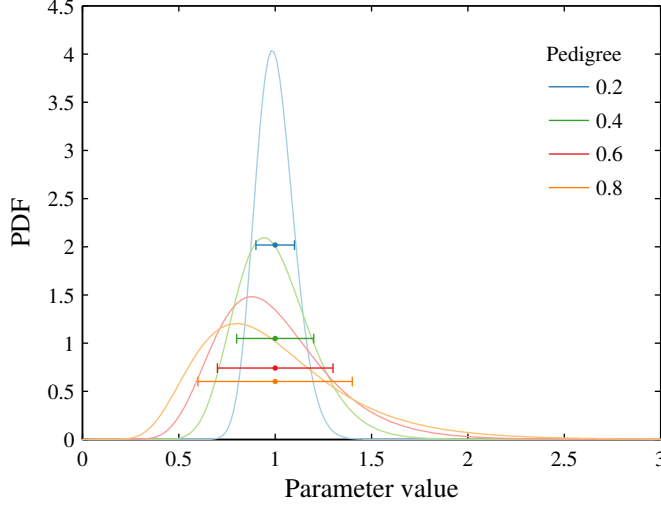
Figure 4: Parameter values were chosen from lognormal probability distribution functions. Shown here are the PDFs for a parameter with mean 1 and pedigrees of 0.2-0.8; the error bars indicate the mean and standard deviation of each PDF.

Ecopath model must by definition covary with other input variables. First, diet composition components for a single predator must sum to 1. This normalization of diet will result in the final set of DC components falling along a normal distribution rather than lognormal.

Multi-stanza groups also require special treatment at this point. In an Ecopath model, biomass groups can represent different life history stages of the same functional group. Ecopath assumes that multi-stanza functional groups represent a stable age-size distribution, and that body size (and by extension biomass and consumption rates) follow a von Bertalanffy growth curve (Christensen & Walters, 2004). The stable age assumption implies that the survivorship l_a at age a is a function of mortality rates (note that in Ecopath, mortality rate Z_i is assumed to be equal to production rate $\frac{P}{B}_i$) and biomass accumulation rate:

$$l_a = \exp\left(-\int_0^a Z_a - a\frac{BA_i}{B_i}\right) \tag{53}$$

and the von Bertalanffy assumption states that weight w_a is related to age by

$$w_a = (1 - \exp(-K_i a))^3 \tag{54}$$

and that consumption is proportional to $w_a^{2/3}$; the growth rate K_i is provided as input by the user for all multi-stanza groups in Ecopath. Based on these assumptions, the proportion of biomass at age a is

$$b_a = \frac{l_a w_a}{\int_0^{a_{max}} l_a w_a} \tag{55}$$

and by extension, the proportion of biomass within a stanza defined between ages a_{smin} and a_{smax} is

$$b_s = \frac{\int_{a_{smin}}^{a_{smax}} l_a w_a}{\int_0^{a_{max}} l_a w_a} \tag{56}$$

21

Likewise, consumption within a stanza is

$$q_s = \frac{\int_{a_{smin}}^{a_{smax}} l_a w_a^{2/3}}{\int_0^{a_{max}} l_a w_a^{2/3}} \tag{57}$$

Therefore, biomass and consumption rates are only set for a single leading stanza group, typically the oldest group, and values for the other stanzas are calculated such that

$$B_{tot} = \frac{B_{s=\text{lead}}}{b_{s=\text{lead}}} \tag{58}$$

$$B_s = B_{tot} b_s \tag{59}$$

$$Q_{tot} = \frac{B_{s=\text{lead}} \frac{Q}{B}_{s=\text{lead}}}{q_{s=\text{lead}}} \tag{60}$$

$$\left(\frac{Q}{B}\right)_s = \frac{Q_{tot} q_s}{B_s} \tag{61}$$

Step 3: Calculate ecotrophic efficiency values for each of the n Ecopath models. Keep only the models that satisfy the mass balance criteria. Balance within an Ecopath model is diagnosed via the ecotrophic efficiency (EE) values for each group, defined as the fraction of net group production that is passed up the food chain to predators. An ecotrophic efficiency value outside the range of 0-1 implies that the system requires an outside sink or source in order to account for all biomass fluxes, and results when input data contradict each other (for example, a predator has a consumption rate that cannot be sustained by the known biomass of its prey). At this point, we keep only the parameter sets that result in a balanced model. For most Ecopath models, this will only be a small fraction of n.

Step 4: Repeat steps 1-3 until n balanced models have been created. By repeating the process of sampling parameters, testing for balance, and keeping only those models that satisfied the balance criteria, we are able to construct an ensemble of Ecopath food web models that incorporate the potential measurement uncertainty.

4   Tables of parameters

Table 1: A description of the 47 functional groups included in the unsimplified version of the food web model. Species listed in the Includes column are not exhaustive, but represent the dominant members of each functional group.

Group	Includes	Details
Sperm whales	sperm whales (*Physeter macrocephalus*)	a very large toothed whale, only mature males are found in the subarctic gyre region, and only during the summer months.
Toothed whales	orcas (*Orcinus orca*)	includes the mammal-eating transient subpopulation and some portion of the piscivororous (and typically more coastal) resident subpopulation

A description of the 47 functional groups included in the unsimplified version of the food web model (continued).

Group	Includes	Details
Fin whales	fin whales (*Balaenoptera physalus*)	a baleen whale, migrates to the gyre during summer months to feed
Sei whales	sei whales (*Balaenoptera boealis*)	a baleen whale, migrates to the gyre during summer months to feed
Northern fur seals	northern fur seals (*Callorhinus ursinus*)	a large fur seal.
Elephant seals	northern elephant seals (*Mirounga angustirostris*)	large seal, migrates biannually between the Alaska Gyre and California breeding beaches.
Dall' s porpoises	Dall' s porpoises (*Phocoenoides dalli*)	a porpoise
Pacific white-sided dolphins	Pacific white-sided dolphins (*Lagenorhynchus obliquidens*)	a dolphin
Northern right whale dolphins	Northern right whale dolphins (*Lissodelphis borealis*)	a small dolphin
Albatross	primarily Black-footed albatross (*Phoebastria nigripes*) and Laysan albatross (*Phoebastria immutabilis*)	large seabirds
Shearwaters	primarily sooty shearwaters (*Puffinus griseus*) and short-tailed shearwaters (*Puffinus tenuirostris*)	medium-sized seabirds, the dominant seabird in the Gulf of Alaska region
Storm Petrels	primarily fork-tailed storm petrels (*Oceanodroma furcata*) and Leach' s storm petrels (*Oceanodroma leucorhoa*)	small seabirds
Kittiwakes	primarily black-legged kittiwakes (*Rissa tridactyla*)	seabirds in the gull family
Fulmars	northern fulmar (*Fulmarus glacialis*)	a seabird
Puffins	primarily tufted puffins (*Fratercula cirrhata*)	a medium-sized seabird
Skuas	primarily south-polar skuas (*Stercorarius maccormicki*)	a large seabird
Jaegers	primarily Pomarine jaegars	seabird, in the skua family
Sharks	salmon sharks (*Lamna ditropis*)	small shark, approximately 2m long, homeothermic
Large gonatid squid	armhook squid (family Gonatidae)	medium-sized squid
Boreal clubhook squid	boreal clubhook squid (*Onychoteuthis borealijaponica*)	a medium-sized squid
Neon flying squid	neon flying squid (*Ommastrephes bartramii*)	a slightly larger squid
Sockeye salmon	sockeye salmon (*Oncorhynchus nerka*)	the most abundant salmon species in the Eastern Gyre, anadromous
Chum salmon	chum salmon (*Oncorhynchus keta*)	the second-most abundant salmon species in the Easterb Gyre, anadromous
Pink salmon	pink salmon (*Oncorhynchus gorbuscha*)	smallest Pacific salmon, anadromous, have a two-year breeding cycle, with even- and odd-year populations not interbreeding
Coho salmon	coho salmon (*Oncorhynchus kisutch*)	a salmon, anadromous
Chinook salmon	Chinook salmon (*Oncorhynchus tshawytscha*)	the largest Pacific salmon, anadromous

A description of the 47 functional groups included in the unsimplified version of the food web model (continued).

Group	Includes	Details
Steelhead	steelhead, or rainbow trout (*Oncorhynchus mykiss*)	salmonid, anadromous
Pomfret	Pacific pomfret (*Brama japonica*)	a large perciform fish
Saury	Pacific saury (*Cololabis saira*)	medium-sized (30-40 cm), highly migratory fish, important commercial fish, especially in Asia
Pelagic forage fish	primarily sticklebacks (*Gasterosteus aculeatus*)	small (4 cm) schooling forage fish
Micronektonic squid	primarily gonatids such as *Berryteuthis anonychus* and *Gonatus onyx*	juvenile squid, few data measurements available
Mesopelagic fish	myctophids, or lanternfishes (family Myctophidae), particularly *Stenobrachius leucopsarus*	small mesopelagic fish
Large jellyfish	phylum Cnidaria	small jellyfish
Ctenophores	phylum Ctenophora	comb jellies, gelatinous
Salps	family Salpidae	planktonic tunicates, gelatinous
Chaetognaths	phylum Chaetognatha	marine worms, gelatinous
Sergestid shrimp	family Sergestidae	shrimp
Miscellaneous predatory zooplankton	mainly Larvaceans and Polychaetes	planktonic tunicates and annelid worms
Amphipods	order Amphipoda	crustacean zooplankton
Pteropods	Thecosomata	planktonic gastropods
Euphausiids	krill (order Euphausiacea)	crustacean zooplankton
Copepods	subclass Copepoda	small crustacean zooplankton
Microzooplankton	any <200 μm	mainly meroplanktonic larva and copepod nauplii
Large phytoplankton	any <5 μm	includes prasinophytes, prymnesiophytes (coccolithophorids), cryptophytes, and cyanobacteria
Small phytoplankton	primarily diatoms	represent large size class, includes silica cycle
DNH3	detritus, dissolved	detritus pool
POM	detritus, particulate	detritus pool

Table 2: Biogeochemical process-related parameters: Primary production

Parameter	Symbol	Group	Value
Ammonium inhibition constant	ψ	PS	1.5 (mmol N m^{-3})$^{-1}$
		PL	1.5 (mmol N m^{-3})$^{-1}$
Half-saturation constant for ammonium	K_{NH_4}	PS	0.1 mmol N m^{-3}
		PL	0.3 mmol N m^{-3}
Half-saturation constant for nitrate	K_{NO_3}	PS	1 mmol N m^{-3}
		PL	3 mmol N m^{-3}
Half-saturation constant for silica	K_{Si}	PL	6 mmol Si m^{-3}
Initial slope of P-I curve	α	PS	0.017 (W m^{-2})$^{-1}$ d^{-1}
		PL	0.016 (W m^{-2})$^{-1}$ d^{-1}
Light dissipation coefficient of seawater	α_1		0.04 m^{-1}
Maximum uptake rate at 0 deg C	V_{max}	PS	0.4 d^{-1}
		PL	0.8 d^{-1}
Phytoplankton self-shading coefficient	α_2		0.04 m^{-1} (mmol N m^{-3})$^{-1}$
Silica to nitrogen ratio	$R_{Si:N}$		2 mmol Si (mmol N)$^{-1}$
Carbon to nitrogen ratio	$R_{C:N}$		6.625 mol C (mol N)$^{-1}$
Temperature coefficient for photosynthesis	K_{gpp}	PS	0.0693 (deg C)$^{-1}$
		PL	0.0693 (deg C)$^{-1}$
Empirical Fe:C function coefficient	b_{Fe}	PS	28.5 (mol C m^{-3})$^{-1}$
		PL	42.6 (mol C m^{-3})$^{-1}$
Empirical Fe:C function power	α_{Fe}	PS	0.21
		PL	0.46
Fraction of iron remineralized	f_{rem}	PS	0.5
		PL	0.5
Half-saturation constant for Fe:C	$K_{Fe:C}$	PS	12 μmol Fe (mol C)$^{-1}$
		PL	16.9 μmol Fe (mol C)$^{-1}$
Timescale for iron uptake	t_{Fe}	PS	1 d
		PL	1 d

Table 3: Biogeochemical process-related parameters: Iron quota model

Parameter	Symbol	Group	Value
Maximum Fe:N ratio	$R_{Fe:Nmax}$	PS	331.25 μmol Fe (mol N)$^{-1}$
		PL	3312.5 μmol Fe (mol N)$^{-1}$
Half-saturation constant for iron	K_{Fe}	PS	0.6 μmol Fe m^{-3}
		PL	3.0 μmol Fe m^{-3}
Half-saturation constant for internal Fe:N ratio	$K_{Fe:N}$	PS	66.25 μmol Fe (mol N)$^{-1}$
		PL	132.5 μmol Fe (mol N)$^{-1}$
Iron uptake factor	$\mu_{Fe:N}$		100 μmol Fe (mol N)$^{-1}$
Background ligand concentration	$Lig_b kg$		1.0 μmol m^{-3}
Half saturation constant for light effect on ligand-binding	K_{Iscav}		1.0 W m^{-2}
Lower limit of ligand binding under low-light conditions	K_{LigLo}		300 m^3 (μmol)$^{-1}$
Upper limit of ligand binding under high-light conditions	K_{LigHi}		0.1 m^3 (μmol)$^{-1}$
Iron scavenging coefficient	α_{scav}		50 yr^{-1}
Fraction of iron remineralized, relative to organic nitrogen	r_{eff}		0.25

Table 4: Biogeochemical process-related parameters: Respiration

Parameter	Symbol	Group	Value
Respiration rate at 0 deg C	Res_0	PS	0.03 d^{-1}
		PL	0.03 d^{-1}
Temperature coefficient for respiration	K_{Res}	PS	0.0519 d^{-1}
		PL	0.0519 d^{-1}

Table 5: Biogeochemical process-related parameters: Extracellular excretion

Parameter	Symbol	Group	Value
Ratio of extracellular excretion to photosynthesis	γ	PS	0.135
		PL	0.135

Table 6: Biogeochemical process-related parameters: Grazing

Parameter	Symbol	Group	Value
Grazing inhibition coefficient	ψ_{gr}	ZP on PL	4.605 (mmol N m^{-3})$^{-1}$
		ZP on ZS	3.01 (mmol N m^{-3})$^{-1}$
Grazing threshhold	B_{thresh}	ZS on PS	0.04 mmol N m^{-3}
		ZL on PS	0.04 mmol N m^{-3}
		ZL on PL	0.04 mmol N m^{-3}
		ZP on PL	0.04 mmol N m^{-3}
		ZL on ZS	0.04 mmol N m^{-3}
		ZP on ZS	0.04 mmol N m^{-3}
		ZP on ZL	0.04 mmol N m^{-3}
Ivlev constant	λ	ZS	1.4 (mmol N m^{-3})$^{-1}$
		ZL	1.4 (mmol N m^{-3})$^{-1}$
		ZP	1.4 (mmol N m^{-3})$^{-1}$
Maximum grazing rate at 0 deg C	g_{max}	ZS on PS	0.8 d^{-1}
		ZL on PS	0.1 d^{-1}
		ZL on PL	0.4 d^{-1}
		ZP on PL	0.2 d^{-1}
		ZL on ZS	0.4 d^{-1}
		ZP on ZS	0.2 d^{-1}
		ZP on ZL	0.2 d^{-1}
Temperature coefficient for grazing	K_{Gra}	ZS	0.0693 (deg C)$^{-1}$
		ZL	0.0693 (deg C)$^{-1}$
		ZP	0.0693 (deg C)$^{-1}$
		gel. zoo.	0.0693 (deg C)$^{-1}$
		pred. zoo.	0.0693 (deg C)$^{-1}$
Mixed layer depth, annual average	MLD		80 m
Mixed layer temperature, annual average	T_{avg}		8.26 deg C

Table 7: Biogeochemical process-related parameters: Egestion and excretion

Parameter	Symbol	Group	Value
Assimilation efficiency	α_{eg}	ZS	0.7
		ZL	0.7
		ZP	0.7
Growth efficiency	β_{eg}	ZS	0.3
		ZL	0.3
		ZP	0.3

Table 8: Biogeochemical process-related parameters: Decomposition

Parameter	Symbol	Group	Value
Decomposition (or nitrification) rate	V_{Dec}	NH_4 to NO_3	0.03 d^{-1}
		PON to NH_4	0.1 d^{-1}
		PON to DON	0.1 d^{-1}
		DON to NH_4	0.02 d^{-1}
		Opal to $SiOH_4$	0.04 d^{-1}
Temperature coefficient for decomposition	K_{Dec}	NH_4 to NO_3	0.0693 $(\deg C)^{-1}$
		PON to NH_4	0.0693 $(\deg C)^{-1}$
		PON to DON	0.0693 $(\deg C)^{-1}$
		DON to NH_4	0.0693 $(\deg C)^{-1}$
		Opal to $SiOH_4$	0.0693 $(\deg C)^{-1}$

Table 9: Biogeochemical process-related parameters: Mortality

Parameter	Symbol	Group	Value
Mortality rate at 0 deg C	Mor_0	PS	0.0585 d^{-1}
		PL	0.029 d^{-1}
		ZS	0.0585 d^{-1}
		ZL	0.0585 d^{-1}
		ZP	0.0585 d^{-1}
Temperature coefficient for mortality	K_{Mor}	PS	0.0693 $(\deg C)^{-1}$
		PL	0.0693 $(\deg C)^{-1}$
		ZS	0.0693 $(\deg C)^{-1}$
		ZL	0.0693 $(\deg C)^{-1}$
		ZP	0.0693 $(\deg C)^{-1}$
Mortality exponent	c	phytoplankton	2.0
		zooplankton	1.5
		nekton	1.0

Table 10: Derived parameters. These parameters vary over time as a function of the state variables from both the physical and biological models.

Parameter Name	Symbol	Definition
Nitrogen limitation	L_N	$\frac{NO_3}{K_{NO_3}+NO_3} \cdot \exp\left(-\psi NH_4\right) + \frac{NH_4}{K_{NH_4}+NH_4}$
Silica limitation	L_{Si}	$\frac{SiOH_4}{K_{SiOH_4}+SiOH_4}$
Iron limitation	L_{Fe}	$\frac{R_{Fe:C}^2}{K_{Fe:C}^2+R_{Fe:C}^2}$
Iron limitation (quota model)	L_{Fe}	$\frac{B_{Fe}}{K_{Fe}+B_{Fe}}$
Iron deficiency	D_{Fe}	$\frac{R_{Fe:N}^2}{K_{Fe:N}^2+R_{Fe:N}^2}$
f-ratio	f	$\frac{\frac{NO_3}{K_{NO_3}+NO_3}\cdot\exp(-\psi NH_4)}{\frac{NO_3}{K_{NO_3}+NO_3}\cdot\exp(-\psi NH_4)+\frac{NH_4}{K_{NH_4}+NH_4}}$
Total nutrient limitation	L_{nut}	$\min\left(L_N, L_{Si}, L_{Fe}\right)$
Total nutrient limitation (quota model)	L_{nut}	$\min\left(L_N, L_{Si}, D_{Fe}\right)$
Light limitation	L_{light}	$1 - \exp\left(\frac{\alpha I_z}{V_{max}}\right)$
Empirical Fe:C ratio	R_{0i}	$b_{Fe,i}Fe_z^{a_{Fe,i}}$
Realized Fe:C ratio	R_i	$\frac{B_{Fe,i}}{B_i \cdot R_{C:N}}$
Realized Fe:N ratio	$R_{Fe:N}$	$\frac{B_{Fe,i}}{B_i}$
Ligand-binding parameter	K_{Lig}	$10^{\left(\log_{10}(K_{LigLo}) - \frac{I_z}{K_{Iscav}+I_z}\right)\left(\log_{10}(K_{LigLo}) - \log_{10}(K_{LigHi})\right)}$

Table 11: Ecopath basic input variables for the 33-group simplified food web, including biomass (B, tons wet weight m^{-2}), production/biomass (PB, yr^{-1}), consumption/biomass (QB, yr^{-1}), ecotrophic efficiency (EE), growth efficiency (GE), and fraction unassimilated (GS)

Group	B		PB		QB		EE		GE		GS
	Value	Ped	Value	Ped	Value	Ped	Value	Ped	Value	Ped	
Albatross	4e-05	0.50	0.05	0.40		0.20		0.05	0.0006128	0.20	0.2
Sperm whales	0.000929	0.50	0.0596	0.40		0.20		0.05	0.009017	0.20	0.2
Sharks	0.05	0.80	0.2	0.60		0.40		0.05	0.01826	0.40	0.2
Neon flying squid	0.45	0.80	2.555	0.60		0.60		0.05	0.4118	0.60	0.2
Toothed whales	2.8e-05	0.50	0.0252	0.40		0.20		0.05	0.002258	0.20	0.2
Elephant seals	0.00043	0.50	0.368	0.40		0.20		0.05	0.03321	0.20	0.2
Seals,dolphins	0.01409	0.50	0.1302	0.40		0.20		0.05	0.004952	0.20	0.2
Boreal clubhook squid	0.012	0.80	2.555	0.60		0.60		0.05	0.35	0.60	0.2
Fulmars	7.4e-05	0.50	0.1	0.40		0.20		0.05	0.0009974	0.20	0.2
Chinook,coho,steelhead	0.02306	0.50	1.123	0.26	7.5	0.26		0.05	0.1499	0.26	0.2
Skuas,Jaegers	9.2e-05	0.50	0.075	0.40		0.20		0.05	0.0007764	0.20	0.2
Pomfret	0.21	0.80	0.75	0.40		0.40		0.05	0.2	0.40	0.2
Puffins,Shearwaters,Storm Petrels	0.000514	0.50	0.1	0.40		0.20		0.05	0.0009411	0.20	0.2
Kittiwakes	5.2e-05	0.50	0.1	0.40		0.20		0.05	0.000813	0.20	0.2
Large gonatid squid	0.03	0.80	2.555	0.60		0.60		0.05	0.35	0.60	0.2
Sockeye,Pink	0.1129	0.50	1.703	0.10		0.10		0.05	0.1437	0.10	0.2
Fin,sei whales	0.03379	0.50	0.02	0.40		0.20		0.05	0.004134	0.20	0.2
Micronektonic squid		0.80	3	0.60		0.70	0.9	0.05	0.2	0.70	0.2
Mesopelagic fish	4.5	0.80	0.9	0.60		0.70		0.05	0.3	0.70	0.2
Pelagic forage fish		0.80	1.5	0.60		0.70	0.9	0.05	0.3	0.70	0.2
Saury	0.45	0.80	1.6	0.60		0.70		0.05	0.2025	0.70	0.2
Chum salmon	0.05414	0.50	1.93	0.10		0.10		0.05	0.133	0.10	0.2
Large jellyfish	4	0.80	3	0.70		0.70		0.05	0.3	0.70	0.2
Chaetognaths	4.129	0.50	7.642	0.70		0.70		0.05	0.3	0.70	0.3
Predatory zooplankton	4.129	0.80	7.642	0.70		0.70		0.05	0.3	0.70	0.3
Sergestid shrimp	4.129	0.80	7.642	0.70		0.70		0.05	0.3	0.70	0.3
Mesozooplankton	15.48	0.80	7.642	0.60		0.60		0.05	0.3	0.60	0.3
Gelatinous zooplankton	3.097	0.50	6.5	0.70		0.70		0.05	0.3	0.70	0.3
Copepods	20.35	0.10	28.07	0.10		0.40		0.05	0.3	0.40	0.3
Microzooplankton	18.41	0.10	46.1	0.10		0.40		0.05	0.3	0.40	0.3
Small phytoplankton	45.54	0.50	85.83	0.10	0	0.40		0.05	0	0.40	0
Large phytoplankton	26.11	0.80	44.27	0.10	0	0.40		0.05	0	0.40	0
DON	100	0.10	0	0.10	0	0.40		0.05	0	0.40	0

Table 12: Ecopath diet fraction input for the 33-group food web model.

Predator	Prey	Diet percentage	Pedigree
Albatross	Neon flying squid	68.60	0.70
	Boreal clubhook squid	1.83	
	Large gonatid squid	4.57	
	Micronektonic squid	5.00	
	Pelagic forage fish	10.00	
	Saury	10.00	
Sperm whales	Neon flying squid	34.30	0.70
	Boreal clubhook squid	0.92	
	Chinook,coho,steelhead	0.05	
	Pomfret	0.49	
	Large gonatid squid	2.29	
	Sockeye,Pink	0.26	
	Micronektonic squid	37.50	
	Mesopelagic fish	10.42	
	Pelagic forage fish	12.60	
	Saury	1.04	
	Chum salmon	0.12	
Sharks	Neon flying squid	26.72	0.80
	Boreal clubhook squid	0.71	
	Chinook,coho,steelhead	1.37	
	Pomfret	12.47	
	Large gonatid squid	1.78	
	Sockeye,Pink	6.71	
	Micronektonic squid	10.00	
	Pelagic forage fish	10.30	
	Saury	26.72	
	Chum salmon	3.21	
Neon flying squid	Neon flying squid	29.50	0.60
	Micronektonic squid	22.30	
	Mesopelagic fish	10.50	
	Pelagic forage fish	31.90	
	Saury	5.80	
Toothed whales	Albatross	0.03	0.70
	Neon flying squid	4.57	
	Elephant seals	0.35	
	Seals,dolphins	11.48	
	Boreal clubhook squid	0.12	
	Fulmars	0.06	
	Chinook,coho,steelhead	0.64	
	Skuas,Jaegers	0.07	
	Pomfret	5.83	
	Puffins,Shearwaters,Storm Petrels	0.42	
	Kittiwakes	0.04	
	Large gonatid squid	0.30	
	Sockeye,Pink	3.14	
	Fin,sei whales	27.54	
	Micronektonic squid	5.00	
	Pelagic forage fish	26.40	
	Saury	12.50	
	Chum salmon	1.50	
Elephant seals	Neon flying squid	18.29	0.70
	Boreal clubhook squid	0.49	
	Chinook,coho,steelhead	0.29	
	Pomfret	5.60	
	Large gonatid squid	1.22	
	Sockeye,Pink	1.43	
	Micronektonic squid	40.00	
	Pelagic forage fish	20.00	
	Saury	12.00	
	Chum salmon	0.68	
Seals,dolphins	Neon flying squid	18.52	0.70

Ecopath diet fraction input for the 33-group food web model (continued).

Predator	Prey	Diet percentage	Pedigree
	Boreal clubhook squid	0.49	
	Chinook,coho,steelhead	0.50	
	Pomfret	4.56	
	Large gonatid squid	1.23	
	Sockeye,Pink	2.45	
	Micronektonic squid	23.06	
	Mesopelagic fish	22.63	
	Pelagic forage fish	15.60	
	Saury	9.76	
	Chum salmon	1.17	
Boreal clubhook squid	Micronektonic squid	99.00	0.60
	Pelagic forage fish	1.00	
Fulmars	Micronektonic squid	96.00	0.70
	Pelagic forage fish	4.00	
Chinook,coho,steelhead	Micronektonic squid	20.57	0.10
	Mesopelagic fish	36.72	
	Pelagic forage fish	36.72	
	Mesozooplankton	5.70	
	Gelatinous zooplankton	0.01	
	Copepods	0.27	
Skuas,Jaegers	Pelagic forage fish	50.00	0.70
	Saury	50.00	
Pomfret	Micronektonic squid	75.00	0.50
	Mesopelagic fish	8.00	
	Saury	4.00	
	Chaetognaths	1.00	
	Predatory zooplankton	1.00	
	Sergestid shrimp	1.00	
	Mesozooplankton	9.00	
	Copepods	1.00	
Puffins,Shearwaters,Storm Petrels	Micronektonic squid	31.01	0.70
	Pelagic forage fish	26.46	
	Saury	26.46	
	Mesozooplankton	9.11	
	Copepods	6.96	
Kittiwakes	Pelagic forage fish	40.00	0.70
	Saury	40.00	
	Mesozooplankton	11.34	
	Copepods	8.66	
Large gonatid squid	Micronektonic squid	33.00	0.60
	Pelagic forage fish	1.00	
	Chaetognaths	4.48	
	Predatory zooplankton	3.44	
	Sergestid shrimp	3.40	
	Mesozooplankton	31.00	
	Copepods	23.68	
Sockeye,Pink	Micronektonic squid	7.04	0.10
	Mesopelagic fish	10.12	
	Pelagic forage fish	10.12	
	Predatory zooplankton	0.14	
	Mesozooplankton	66.82	
	Gelatinous zooplankton	2.71	
	Copepods	3.04	
Fin,sei whales	Neon flying squid	2.29	0.70
	Boreal clubhook squid	0.06	
	Chinook,coho,steelhead	0.03	
	Pomfret	0.29	
	Large gonatid squid	0.15	
	Sockeye,Pink	0.16	
	Micronektonic squid	2.50	
	Mesopelagic fish	6.25	

Ecopath diet fraction input for the 33-group food web model (continued).

| Predator	Prey	Diet percentage	Pedigree
	Pelagic forage fish	7.60	
	Saury	0.62	
	Chum salmon	0.08	
	Chaetognaths	5.44	
	Predatory zooplankton	4.17	
	Sergestid shrimp	4.12	
	Mesozooplankton	37.57	
	Copepods	28.70	
Micronektonic squid	Micronektonic squid	5.00	0.70
	Chaetognaths	6.46	
	Predatory zooplankton	4.96	
	Sergestid shrimp	4.89	
	Mesozooplankton	44.62	
	Copepods	34.08	
Mesopelagic fish	Chaetognaths	15.00	0.70
	Predatory zooplankton	3.00	
	Sergestid shrimp	3.00	
	Mesozooplankton	44.20	
	Copepods	34.80	
Pelagic forage fish	Chaetognaths	6.79	0.70
	Predatory zooplankton	5.22	
	Sergestid shrimp	5.15	
	Mesozooplankton	46.97	
	Copepods	35.88	
Saury	Chaetognaths	5.30	0.70
	Predatory zooplankton	4.07	
	Sergestid shrimp	4.01	
	Mesozooplankton	36.62	
	Copepods	50.00	
Chum salmon	Micronektonic squid	3.93	0.10
	Mesopelagic fish	0.80	
	Pelagic forage fish	0.80	
	Chaetognaths	0.04	
	Predatory zooplankton	1.47	
	Mesozooplankton	22.57	
	Gelatinous zooplankton	40.57	
	Copepods	29.81	
Large jellyfish	Chaetognaths	3.16	0.70
	Predatory zooplankton	2.43	
	Sergestid shrimp	2.39	
	Mesozooplankton	21.83	
	Gelatinous zooplankton	8.19	
	Copepods	62.00	
Chaetognaths	Mesozooplankton	20.00	0.70
	Copepods	80.00	
Predatory zooplankton	Mesozooplankton	20.00	0.70
	Copepods	80.00	
Sergestid shrimp	Mesozooplankton	20.00	0.70
	Copepods	80.00	
Mesozooplankton	Copepods	40.00	0.57
	Microzooplankton	40.00	
	Large phytoplankton	20.00	
Gelatinous zooplankton	Copepods	25.00	0.70
	Microzooplankton	25.00	
	Large phytoplankton	50.00	
Copepods	Microzooplankton	30.00	0.30
	Small phytoplankton	30.00	
	Large phytoplankton	40.00	
Microzooplankton	Small phytoplankton	100.00	0.30

Table 13: Ecopath-derived parameters for living state variables, including mass-balanced biomass (B^*, mol N m^{-2}), mass-balanced mortality flux per unit biomass (M_0, s^{-1}), growth efficiency (GE), and unassimilation fraction (GS). The histogram columns indicate the distribution of values across ensemble members, with the column width ranging from 0 to 3.5 times the mean value.

| Group	B*		M0		GE		GS
	mean	histogram	mean	histogram	mean	histogram	
Albatross	1.54e-08		1.51e-09		0.001		0.2
Sperm whales	3.36e-07		1.89e-09		0.009		0.2
Sharks	1.74e-05		5.98e-09		0.019		0.2
Neon flying squid	1.69e-04		1.95e-08		0.504		0.2
Toothed whales	1.08e-08		7.80e-10		0.002		0.2
Elephant seals	1.64e-07		1.13e-08		0.033		0.2
Seals,dolphins	5.36e-06		4.04e-09		0.005		0.2
Boreal clubhook squid	4.40e-06		6.54e-08		0.342		0.2
Fulmars	2.76e-08		3.06e-09		0.001		0.2
Chinook,coho,steelhead	8.67e-06		2.29e-08		0.155		0.2
Skuas,Jaegers	3.46e-08		2.28e-09		0.001		0.2
Pomfret	8.60e-05		1.28e-08		0.205		0.2
Puffins,Shearwaters,Storm Petrels	1.90e-07		3.08e-09		0.001		0.2
Kittiwakes	1.84e-08		3.18e-09		0.001		0.2
Large gonatid squid	1.12e-05		5.71e-08		0.336		0.2
Sockeye,Pink	4.15e-05		4.12e-08		0.145		0.2
Fin,sei whales	1.25e-05		5.57e-10		0.004		0.2
Micronektonic squid	3.99e-04		9.34e-09		0.200		0.2
Mesopelagic fish	1.63e-03		2.35e-08		0.291		0.2
Pelagic forage fish	3.60e-04		4.99e-09		0.301		0.2
Saury	1.81e-04		2.65e-08		0.203		0.2
Chum salmon	2.04e-05		4.85e-08		0.133		0.2
Large jellyfish	1.44e-03		8.94e-08		0.306		0.2
Chaetognaths	1.48e-03		1.77e-07		0.325		0.3
Predatory zooplankton	1.38e-03		1.92e-07		0.320		0.3
Sergestid shrimp	1.46e-03		2.18e-07		0.330		0.3
Mesozooplankton	5.93e-03		7.51e-08		0.320		0.3
Gelatinous zooplankton	1.18e-03		1.60e-07		0.313		0.3
Copepods	7.62e-03		2.12e-07		0.330		0.3
Microzooplankton	6.95e-03		2.80e-07		0.308		0.3
Small phytoplankton	1.92e-02		5.79e-07		0.000		0.0
Large phytoplankton	1.12e-02		4.71e-07		0.000		0.0

Table 14: Ecopath-derived parameters for predator-prey processes, including mass-balanced consumption rate (Q^*, mol N m^{-2} s^{-1}), top-down control parameter (X), bottom-up control parameter (D), and functional response exponent (θ). The histogram column indicates the distribution of values across ensemble members, with the column width ranging from 0 to 3.5 times the mean value.

| Predator	Prey	Q* mean	Q* histogram	X	D	θ
Albatross	Neon flying squid	2.64e-14		2.0	1000.0	2.0
Albatross	Boreal clubhook squid	7.52e-16		2.0	1000.0	2.0
Albatross	Large gonatid squid	1.98e-15		2.0	1000.0	2.0
Albatross	Micronektonic squid	2.10e-15		2.0	1000.0	2.0
Albatross	Pelagic forage fish	4.55e-15		2.0	1000.0	2.0
Albatross	Saury	4.35e-15		2.0	1000.0	2.0
Sperm whales	Neon flying squid	2.53e-14		2.0	1000.0	2.0
Sperm whales	Boreal clubhook squid	6.56e-16		2.0	1000.0	2.0
Sperm whales	Chinook,coho,steelhead	3.92e-17		2.0	1000.0	2.0
Sperm whales	Pomfret	3.54e-16		2.0	1000.0	2.0
Sperm whales	Large gonatid squid	1.70e-15		2.0	1000.0	2.0
Sperm whales	Sockeye,Pink	1.89e-16		2.0	1000.0	2.0
Sperm whales	Micronektonic squid	2.52e-14		2.0	1000.0	2.0
Sperm whales	Mesopelagic fish	7.67e-15		2.0	1000.0	2.0
Sperm whales	Pelagic forage fish	8.47e-15		2.0	1000.0	2.0
Sperm whales	Saury	7.41e-16		2.0	1000.0	2.0
Sperm whales	Chum salmon	9.11e-17		2.0	1000.0	2.0
Sharks	Neon flying squid	1.48e-12		2.0	1000.0	2.0
Sharks	Boreal clubhook squid	4.06e-14		2.0	1000.0	2.0
Sharks	Chinook,coho,steelhead	7.94e-14		2.0	1000.0	2.0
Sharks	Pomfret	6.83e-13		2.0	1000.0	2.0
Sharks	Large gonatid squid	1.00e-13		2.0	1000.0	2.0
Sharks	Sockeye,Pink	3.83e-13		2.0	1000.0	2.0
Sharks	Micronektonic squid	6.04e-13		2.0	1000.0	2.0
Sharks	Pelagic forage fish	5.95e-13		2.0	1000.0	2.0
Sharks	Saury	1.51e-12		2.0	1000.0	2.0
Sharks	Chum salmon	1.87e-13		2.0	1000.0	2.0
Neon flying squid	Neon flying squid	8.19e-12		2.0	1000.0	2.0
Neon flying squid	Micronektonic squid	7.06e-12		2.0	1000.0	2.0
Neon flying squid	Mesopelagic fish	3.33e-12		2.0	1000.0	2.0
Neon flying squid	Pelagic forage fish	9.59e-12		2.0	1000.0	2.0
Neon flying squid	Saury	1.62e-12		2.0	1000.0	2.0
Toothed whales	Albatross	1.13e-18		2.0	1000.0	2.0
Toothed whales	Neon flying squid	1.67e-16		2.0	1000.0	2.0
Toothed whales	Elephant seals	1.33e-17		2.0	1000.0	2.0
Toothed whales	Seals,dolphins	4.21e-16		2.0	1000.0	2.0
Toothed whales	Boreal clubhook squid	4.53e-18		2.0	1000.0	2.0
Toothed whales	Fulmars	2.24e-18		2.0	1000.0	2.0
Toothed whales	Chinook,coho,steelhead	2.42e-17		2.0	1000.0	2.0
Toothed whales	Skuas,Jaegers	2.86e-18		2.0	1000.0	2.0
Toothed whales	Pomfret	2.21e-16		2.0	1000.0	2.0
Toothed whales	Puffins,Shearwaters,Storm Petrels	1.62e-17		2.0	1000.0	2.0
Toothed whales	Kittiwakes	1.62e-18		2.0	1000.0	2.0
Toothed whales	Large gonatid squid	1.11e-17		2.0	1000.0	2.0
Toothed whales	Sockeye,Pink	1.18e-16		2.0	1000.0	2.0
Toothed whales	Fin,sei whales	1.03e-15		2.0	1000.0	2.0
Toothed whales	Micronektonic squid	1.83e-16		2.0	1000.0	2.0
Toothed whales	Pelagic forage fish	1.03e-15		2.0	1000.0	2.0
Toothed whales	Saury	4.38e-16		2.0	1000.0	2.0
Toothed whales	Chum salmon	5.73e-17		2.0	1000.0	2.0
Elephant seals	Neon flying squid	1.02e-14		2.0	1000.0	2.0
Elephant seals	Boreal clubhook squid	2.69e-16		2.0	1000.0	2.0
Elephant seals	Chinook,coho,steelhead	1.61e-16		2.0	1000.0	2.0
Elephant seals	Pomfret	3.11e-15		2.0	1000.0	2.0
Elephant seals	Large gonatid squid	6.87e-16		2.0	1000.0	2.0

Ecopath-derived parameters for predator-prey processes (continued).

Predator	Prey	Q* mean	Q* histogram	X	D	θ
Elephant seals	Sockeye,Pink	8.02e-16		2.0	1000.0	2.0
Elephant seals	Micronektonic squid	2.38e-14		2.0	1000.0	2.0
Elephant seals	Pelagic forage fish	9.99e-15		2.0	1000.0	2.0
Elephant seals	Saury	6.75e-15		2.0	1000.0	2.0
Elephant seals	Chum salmon	3.82e-16		2.0	1000.0	2.0
Seals,dolphins	Neon flying squid	8.66e-13		2.0	1000.0	2.0
Seals,dolphins	Boreal clubhook squid	2.34e-14		2.0	1000.0	2.0
Seals,dolphins	Chinook,coho,steelhead	2.31e-14		2.0	1000.0	2.0
Seals,dolphins	Pomfret	2.06e-13		2.0	1000.0	2.0
Seals,dolphins	Large gonatid squid	5.28e-14		2.0	1000.0	2.0
Seals,dolphins	Sockeye,Pink	1.13e-13		2.0	1000.0	2.0
Seals,dolphins	Micronektonic squid	1.02e-12		2.0	1000.0	2.0
Seals,dolphins	Mesopelagic fish	1.05e-12		2.0	1000.0	2.0
Seals,dolphins	Pelagic forage fish	6.77e-13		2.0	1000.0	2.0
Seals,dolphins	Saury	4.55e-13		2.0	1000.0	2.0
Seals,dolphins	Chum salmon	5.51e-14		2.0	1000.0	2.0
Boreal clubhook squid	Micronektonic squid	1.10e-12		2.0	1000.0	2.0
Boreal clubhook squid	Pelagic forage fish	1.34e-14		2.0	1000.0	2.0
Fulmars	Micronektonic squid	8.55e-14		2.0	1000.0	2.0
Fulmars	Pelagic forage fish	3.88e-15		2.0	1000.0	2.0
Chinook,coho,steelhead	Micronektonic squid	4.05e-12		2.0	1000.0	2.0
Chinook,coho,steelhead	Mesopelagic fish	7.61e-13		2.0	1000.0	2.0
Chinook,coho,steelhead	Pelagic forage fish	7.49e-13		2.0	1000.0	2.0
Chinook,coho,steelhead	Mesozooplankton	1.09e-13		2.0	1000.0	2.0
Chinook,coho,steelhead	Gelatinous zooplankton	2.86e-16		2.0	1000.0	2.0
Chinook,coho,steelhead	Copepods	5.65e-15		2.0	1000.0	2.0
Skuas,Jaegers	Pelagic forage fish	5.31e-14		2.0	1000.0	2.0
Skuas,Jaegers	Saury	5.20e-14		2.0	1000.0	2.0
Pomfret	Micronektonic squid	7.85e-12		2.0	1000.0	2.0
Pomfret	Mesopelagic fish	8.35e-13		2.0	1000.0	2.0
Pomfret	Saury	3.99e-13		2.0	1000.0	2.0
Pomfret	Chaetognaths	1.06e-13		2.0	1000.0	2.0
Pomfret	Predatory zooplankton	1.04e-13		2.0	1000.0	2.0
Pomfret	Sergestid shrimp	1.04e-13		2.0	1000.0	2.0
Pomfret	Mesozooplankton	9.59e-13		2.0	1000.0	2.0
Pomfret	Copepods	1.06e-13		2.0	1000.0	2.0
Puffins,Shearwaters,Storm Petrels	Micronektonic squid	2.06e-13		2.0	1000.0	2.0
Puffins,Shearwaters,Storm Petrels	Pelagic forage fish	1.78e-13		2.0	1000.0	2.0
Puffins,Shearwaters,Storm Petrels	Saury	1.65e-13		2.0	1000.0	2.0
Puffins,Shearwaters,Storm Petrels	Mesozooplankton	5.68e-14		2.0	1000.0	2.0
Puffins,Shearwaters,Storm Petrels	Copepods	4.50e-14		2.0	1000.0	2.0
Kittiwakes	Pelagic forage fish	3.02e-14		2.0	1000.0	2.0
Kittiwakes	Saury	3.05e-14		2.0	1000.0	2.0
Kittiwakes	Mesozooplankton	8.43e-15		2.0	1000.0	2.0
Kittiwakes	Copepods	6.57e-15		2.0	1000.0	2.0
Large gonatid squid	Micronektonic squid	8.74e-13		2.0	1000.0	2.0
Large gonatid squid	Pelagic forage fish	2.83e-14		2.0	1000.0	2.0
Large gonatid squid	Chaetognaths	1.25e-13		2.0	1000.0	2.0
Large gonatid squid	Predatory zooplankton	1.04e-13		2.0	1000.0	2.0
Large gonatid squid	Sergestid shrimp	9.54e-14		2.0	1000.0	2.0
Large gonatid squid	Mesozooplankton	8.34e-13		2.0	1000.0	2.0
Large gonatid squid	Copepods	6.58e-13		2.0	1000.0	2.0
Sockeye,Pink	Micronektonic squid	1.16e-12		2.0	1000.0	2.0
Sockeye,Pink	Mesopelagic fish	1.73e-12		2.0	1000.0	2.0
Sockeye,Pink	Pelagic forage fish	1.60e-12		2.0	1000.0	2.0
Sockeye,Pink	Predatory zooplankton	2.09e-14		2.0	1000.0	2.0
Sockeye,Pink	Mesozooplankton	1.01e-11		2.0	1000.0	2.0
Sockeye,Pink	Gelatinous zooplankton	4.17e-13		2.0	1000.0	2.0
Sockeye,Pink	Copepods	4.87e-13		2.0	1000.0	2.0

Ecopath-derived parameters for predator-prey processes (continued).

Predator	Prey	Q*		X	D	θ
		mean	histogram			
Fin,sei whales	Neon flying squid	4.63e-14		2.0	1000.0	2.0
Fin,sei whales	Boreal clubhook squid	1.20e-15		2.0	1000.0	2.0
Fin,sei whales	Chinook,coho,steelhead	6.25e-16		2.0	1000.0	2.0
Fin,sei whales	Pomfret	5.86e-15		2.0	1000.0	2.0
Fin,sei whales	Large gonatid squid	2.98e-15		2.0	1000.0	2.0
Fin,sei whales	Sockeye,Pink	3.04e-15		2.0	1000.0	2.0
Fin,sei whales	Micronektonic squid	5.00e-14		2.0	1000.0	2.0
Fin,sei whales	Mesopelagic fish	1.22e-13		2.0	1000.0	2.0
Fin,sei whales	Pelagic forage fish	1.46e-13		2.0	1000.0	2.0
Fin,sei whales	Saury	1.35e-14		2.0	1000.0	2.0
Fin,sei whales	Chum salmon	1.46e-15		2.0	1000.0	2.0
Fin,sei whales	Chaetognaths	1.02e-13		2.0	1000.0	2.0
Fin,sei whales	Predatory zooplankton	8.39e-14		2.0	1000.0	2.0
Fin,sei whales	Sergestid shrimp	7.50e-14		2.0	1000.0	2.0
Fin,sei whales	Mesozooplankton	7.16e-13		2.0	1000.0	2.0
Fin,sei whales	Copepods	5.52e-13		2.0	1000.0	2.0
Micronektonic squid	Micronektonic squid	1.12e-11		2.0	1000.0	2.0
Micronektonic squid	Chaetognaths	1.32e-11		2.0	1000.0	2.0
Micronektonic squid	Predatory zooplankton	1.08e-11		2.0	1000.0	2.0
Micronektonic squid	Sergestid shrimp	1.01e-11		2.0	1000.0	2.0
Micronektonic squid	Mesozooplankton	9.18e-11		2.0	1000.0	2.0
Micronektonic squid	Copepods	7.17e-11		2.0	1000.0	2.0
Mesopelagic fish	Chaetognaths	2.58e-11		2.0	1000.0	2.0
Mesopelagic fish	Predatory zooplankton	5.22e-12		2.0	1000.0	2.0
Mesopelagic fish	Sergestid shrimp	5.40e-12		2.0	1000.0	2.0
Mesopelagic fish	Mesozooplankton	7.85e-11		2.0	1000.0	2.0
Mesopelagic fish	Copepods	6.19e-11		2.0	1000.0	2.0
Pelagic forage fish	Chaetognaths	4.06e-12		2.0	1000.0	2.0
Pelagic forage fish	Predatory zooplankton	2.99e-12		2.0	1000.0	2.0
Pelagic forage fish	Sergestid shrimp	2.83e-12		2.0	1000.0	2.0
Pelagic forage fish	Mesozooplankton	2.80e-11		2.0	1000.0	2.0
Pelagic forage fish	Copepods	1.99e-11		2.0	1000.0	2.0
Saury	Chaetognaths	2.89e-12		2.0	1000.0	2.0
Saury	Predatory zooplankton	2.18e-12		2.0	1000.0	2.0
Saury	Sergestid shrimp	2.34e-12		2.0	1000.0	2.0
Saury	Mesozooplankton	2.00e-11		2.0	1000.0	2.0
Saury	Copepods	2.76e-11		2.0	1000.0	2.0
Chum salmon	Micronektonic squid	3.78e-13		2.0	1000.0	2.0
Chum salmon	Mesopelagic fish	8.61e-14		2.0	1000.0	2.0
Chum salmon	Pelagic forage fish	7.60e-14		2.0	1000.0	2.0
Chum salmon	Chaetognaths	3.89e-15		2.0	1000.0	2.0
Chum salmon	Predatory zooplankton	1.45e-13		2.0	1000.0	2.0
Chum salmon	Mesozooplankton	2.10e-12		2.0	1000.0	2.0
Chum salmon	Gelatinous zooplankton	3.79e-12		2.0	1000.0	2.0
Chum salmon	Copepods	2.87e-12		2.0	1000.0	2.0
Large jellyfish	Chaetognaths	1.33e-11		2.0	1000.0	2.0
Large jellyfish	Predatory zooplankton	1.15e-11		2.0	1000.0	2.0
Large jellyfish	Sergestid shrimp	1.10e-11		2.0	1000.0	2.0
Large jellyfish	Mesozooplankton	9.25e-11		2.0	1000.0	2.0
Large jellyfish	Gelatinous zooplankton	3.80e-11		2.0	1000.0	2.0
Large jellyfish	Copepods	2.85e-10		2.0	1000.0	2.0
Chaetognaths	Mesozooplankton	2.08e-10		1000.0	14.7	2.0
Chaetognaths	Copepods	8.71e-10		1000.0	3.3	2.0
Predatory zooplankton	Mesozooplankton	1.93e-10		1000.0	19.6	2.0
Predatory zooplankton	Copepods	8.24e-10		1000.0	7.8	2.0
Sergestid shrimp	Mesozooplankton	2.32e-10		1000.0	13.3	2.0
Sergestid shrimp	Copepods	9.38e-10		1000.0	3.7	2.0
Mesozooplankton	Copepods	1.86e-09		1000.0	22.2	2.0
Mesozooplankton	Microzooplankton	1.88e-09		1000.0	19.8	2.0

Ecopath-derived parameters for predator-prey processes (continued).

Predator	Prey	Q*		X	D	θ
		mean	histogram			
Mesozooplankton	Large phytoplankton	9.30e-10		1000.0	32.2	2.0
Gelatinous zooplankton	Copepods	2.11e-10		1000.0	12.4	2.0
Gelatinous zooplankton	Microzooplankton	2.18e-10		1000.0	10.8	2.0
Gelatinous zooplankton	Large phytoplankton	4.20e-10		1000.0	8.6	2.0
Copepods	Microzooplankton	6.13e-09		1000.0	10.7	2.0
Copepods	Small phytoplankton	6.57e-09		1000.0	1.8	2.0
Copepods	Large phytoplankton	8.46e-09		1000.0	7.4	2.0
Microzooplankton	Small phytoplankton	3.39e-08		1000.0	2.9	2.0

References

Aydin KY, McFarlane GA, King JR, Megrey BA (2003) The BASS/MODEL report on trophic models of the Subarctic Pacific Basin ecosystems. PICES Sci Rep 25(25)

Baker KS, Frouin R (1987) Relation between photosynthetically available radiation and total insolation at the ocean surface under clear skies. Limnol Oceanogr 32(6):1370–1377

Christensen V, Walters CJ (2004) Ecopath with Ecosim: methods, capabilities and limitations. Ecol Modell 172:109–139

Christensen V, Walters CJ, Pauly D (2005) Ecopath with Ecosim:A User's Guide

Eslinger DL, Kashiwai MB, Kishi MJ, Megrey BA, Ware DM, Werner FE (2000) MODEL Task Team Workshop Report-Final report of the international Workshop to develop a prototype lower trophic level model for comparison of different marine ecosystems in the North pacific. PICES Sci Rep 15

Fan SM (2008) Photochemical and biochemical controls on reactive oxygen and iron speciation in the pelagic surface ocean. Mar Chem 109(1-2):152–164

Friehe CA, Schmitt KF (1976) Parameterization of air-sea interface fluxes of sensible heat and moisture by the bulk aerodynamic formulas. J Phys Oceanogr 6(6):801–809

Galperin B, Kantha L, Hassid S, Rosati A (1988) A quasi-equilibrium turbulent energy model for geophysical flows. J Atmos Sci 45:55–62

Goldblatt R, Mackas D, Lewis a (1999) Mesozooplankton community characteristics in the NE subarctic Pacific. Deep Sea Res Part II Top Stud Oceanogr 46(11-12):2619–2644

Harris R, Wiebe P, Lenz J, Skjoldal HR, Huntley M (2000) Zooplankton Methodology Manual. Elsevier Academic Press

Harrison PJ, Whitney Fa, Tsuda A, Saito H, Tadokoro K (2004) Nutrient and Plankton Dynamics in the NE and NW Gyres of the Subarctic Pacific Ocean. J Oceanogr 60(1):93–117

Johnson KS, Gordon R, Coale KH (1997) What controls dissolved iron concentrations in the world ocean? Mar Chem 57(3-4):137–161

Johnson M, Moore L, Ylvisaker D (1990) Minimax and maximin distance designs. J Stat Plan Inference 26(2):131–148

Kearney KA (2012) An analysis of marine ecosystem dynamics through development of a coupled physical-biogeochemical-fisheries food web model. Ph.D. thesis, Princeton University

Kearney KA, Stock C, Aydin K, Sarmiento JL (2012) Coupling planktonic ecosystem and fisheries food web models for a pelagic ecosystem: Description and validation for the subarctic Pacific. Ecol Modell 237-238:43–62

Kearney KA, Stock C, Sarmiento JL (2013) Amplification and attenuation of increased primary production in a marine food web. Mar Ecol Prog Ser 491:1–14

Kishi M, Kashiwai M, Ware D, Megrey B, Eslinger D, Werner F, Noguchiaita M, Azumaya T, Fujii M, Hashimoto S (2007) NEMURO- a lower trophic level model for the North Pacific marine ecosystem. Ecol Modell 202(1-2):12–25

Large WG, Pond S (1981) Open ocean momentum flux measurements in moderate to strong winds. J Phys Oceanogr 11(3):324–336

Marshall J, Plumb RA (2008) Atmosphere, Ocean and Climate Dynamics: An Introductory Text. Academic Press

Megrey B, Kishi M, Kashiwai M, Ware D, Eslinger D, Werner F (2000) PICES Lower trophic level modeling workshop, Nemuro. PICES Press 8(2):18–22

Mellor G, Blumberg A (2004) Wave breaking and ocean surface layer thermal response. J Phys Oceanogr 34(3):693–698

Mellor GL (2001) One-dimensional, ocean surface layer modeling: A problem and a solution. J Phys Oceanogr 31(3):790–809

Mellor GL (2004) User's guide for a three-dimensional, primitive equation, numerical ocean model. Atmospheric and Oceanic Sciences Program, Princeton University

Mellor GL, Yamada T (1982) Development of a turbulence closure model for geophysical fluid problems. Rev Geophys Sp Phys 20(4):851–875

Pauly D, Christensen V, Haggan N (1996) Mass-balance models of north-eastern Pacific ecosystems. Fish Cent Res Reports 4(1):131

Reed R (1977) On estimating insolation over the ocean. J Phys Oceanogr 7:482–485

Reeve MR, Walter MA, Ikeda T (1978) Laboratory studies of ingestion and food utilization lobate and tentaculate ctenophores. Limnol Oceanogr 23(4):740–751

Reeve MR, Syms MA, Kremer P (1989) Growth dynamics of a ctenophore (Mnemiopsis) in relation to variable food supply. I. Carbon biomass, feeding, egg production, growth and assimilation efficiency. J Plankton Res 11(3):535–552

Simpson JJ, Paulson CA (1979) Mid-ocean observations of atmospheric radiation. Q J R Meteorol Soc 105(444):487–502

Stock CA, Dunne JP, John J (in press) Global-scale carbon and energy flows through the planktonic food web: an analysis with a coupled physical-biological model. Prog Oceanogr

Umoh JU, Thompson KR (1994) Surface heat flux, horizontal advection, and the seasonal evolution of water temperature on the Scotian Shelf. J Geophys Res 99(C10):20403–20416

Williams B (2006) Hydrobiological modeling

Yuan J, Shiller AM (2001) The distribution of hydrogen peroxide in the southern and central Atlantic ocean. Deep Sea Res Part II Top Stud Oceanogr 48(13):2947–2970